



High-fidelity coupled Monte Carlo neutron transport and thermal-hydraulic simulations using Serpent 2/SUBCHANFLOW



Miriam Daeubler ^{a,*}, Aleksandar Ivanov ^a, Bart L. Sjenitzer ^b, Victor Sanchez ^a, Robert Stieglitz ^a, Rafael Macian-Juan ^c

^a Karlsruhe Institute of Technology, Institute of Neutron Physics and Reactor Technology, Hermann-von-Helmholtz-Platz 1, 76344 Eggenstein-Leopoldshafen, Germany

^b SCK-CEN, Belgian Nuclear Research Center, Boeretang 200, BE-2400 Mol, Belgium

^c Technical University of Munich, Department of Nuclear Engineering, Boltzmannstrasse 15, 85748 Garching, Germany

ARTICLE INFO

Article history:

Received 26 October 2014

Received in revised form 4 March 2015

Accepted 21 March 2015

Available online 8 April 2015

Keywords:

Serpent
SUBCHANFLOW
Internal coupling
Multi-physics
High-fidelity

ABSTRACT

Efforts to develop high-fidelity, *in silico* or *ab initio*, high performance multi-physics tools are undertaken by many groups due to the availability of relatively cheap, large-scale parallel computers. To this end, an internal coupling between the Monte Carlo reactor physics code Serpent 2 and the sub-channel code SUBCHANFLOW has been developed. The coupled code system is intended to serve as reference for deterministic reactor dynamics code developments in the future. It exploits the fact that Serpent was conceived as a lattice code for such deterministic tools. The coupling utilizes Serpent's recently introduced universal multi-physics interface. With the multi-physics interface enabled, Serpent treats temperature dependence of nuclear data using the target motion sampling method. Since the target motion sampling methodology cannot be applied to thermal bound-atom scattering or unresolved resonances, a stochastic mixing fall back algorithm to enable the simulation of thermal reactors has been implemented. The developed coupled code is verified by code-to-code comparison with an external coupling of the Monte Carlo tool TRIPOLI4 and SUBCHANFLOW as well as the internally coupled code MCNP5/SUBCHANFLOW. Simulation results of all code systems were found to be in good agreement. Thereafter, the second exercise of the OECD/NEA and U.S. NRC PWR MOX/UO₂ core transient benchmark is studied to demonstrate that Serpent 2/SUBCHANFLOW may be employed to analyze realistic, industry-like cases such as a full PWR core under hot full power conditions in a reasonable amount of time. The obtained simulation results are compared to known benchmark solutions and the numerical performance of Serpent 2/SUBCHANFLOW is analyzed to assess the feasibility of routine application. While Serpent 2/SUBCHANFLOW's performance in terms of physics and numerical efficiency is found to be generally satisfactory, options to further improve the coupled tool concerning both aspects are discussed. Afterwards, first efforts to validate Serpent 2/SUBCHANFLOW using the hot zero power state of the cycle 1 of the BEAVRS benchmark are presented.

© 2015 Elsevier Ltd. All rights reserved.

1. Introduction

Worldwide efforts to develop high-fidelity reactor simulation tools to be run on large-scale parallel computers for nuclear reactor design, optimization and safety analysis are undertaken. Developers intend to apply these tools instead of industrial standard Best-Estimate (BE) methods in the future. At the last International Conference on Mathematics and Computation (M&C), the large number of challenges one is facing developing such high-fidelity, *in silico* or *ab initio* tools has been summarized

by Smith and Forget (2013). Most current efforts focus on pin-resolved neutron transport, thermal-hydraulics and mechanics simulations. Pin-resolved means here that all fuel rods are modeled explicitly without any significant simplifications in terms of geometry and materials. However, none of the tool prototypes known to the authors has yet reached a level of maturity as envisioned by Smith and Forget.

Groups working on high-fidelity reactor simulators employ both deterministic and Monte Carlo methods to solve the neutron transport problem. For example, the full core deterministic transport code nTRACER and the sub-channel code MATRA have been employed to perform core follow calculations for a Korean OPR1000 reactor (Jung et al., 2013). Furthermore, nTRACER has

* Corresponding author.

E-mail address: miriam.daeubler@kit.edu (M. Daeubler).

been used to study a simplified version of cycle 1 and 2 of the BEAVRS core (Ryu et al., 2014). Besides sub-channel thermal-hydraulic tools, computational fluid dynamics (CFD) codes have been used together with deterministic neutron transport codes to analyze a pressurized water reactor (PWR) core with quarter symmetry under steady-state conditions (Weber et al., 2007; Kochunas et al., 2012). Many groups couple Monte Carlo (MC) neutron transport methods to thermal-hydraulic tools (Espel et al., 2013; Li and Wang, 2012; Bernnat et al., 2012; Vazquez et al., 2012; Ivanov et al., 2013, 2014; Gill et al., 2014). Most of these coupling efforts utilize the MC code MCNP. The studied geometries vary from single fuel assemblies to full cores but so does the spatial resolution of the corresponding thermal-hydraulics model. The simulation of a hot full power (HFP) state of a full PWR core was performed by Bernnat et al. employing channel level thermal-hydraulics (Bernnat et al., 2012). Kelly et al. (2014) were the first to perform a core follow calculation for a simplified version of the first cycle of the PWR described in the BEAVRS benchmark.

The overall goal of this work is to obtain reference solutions to foster improving deterministic reactor dynamics codes, especially low order deterministic transport (SP_3 or diffusion) based ones such as the pin-homogenized simulator DYNSUB developed at KIT (Gomez-Torres et al., 2012a,b). As a first step, a coupled Monte Carlo neutron transport and thermal-hydraulics multi-physics tool is to be developed. Unlike MCNP, the Monte Carlo code Serpent developed by VTT Technical Research Center of Finland (Leppänen, 2013b) was originally designed and optimized to be used as a lattice code to generate effective few-group cross section libraries for such deterministic tools. While Serpent's current scope covers most reactor physics applications, it still offers the unique possibility to easily provide a reference solution and few-group cross section sets for a given problem to a deterministic reactor simulator eliminating the need to use a third tool, a classical deterministic lattice code. The latter would only introduce further sources of errors and complicate the performance analysis of the deterministic reactor simulator. Consequently, Serpent was chosen as stochastic neutron transport code in this work. Because of its superior functionality it was decided to use the Serpent 2 beta (SSS2) instead of the official Serpent 1 release. Though conceptually a high-fidelity, *in silico* or *ab initio* multi-physics tool should employ CFD as the thermal-hydraulics model with the least approximations, the authors feel that CFD in the nuclear engineering field is not yet mature enough and its computational cost is too high. To allow for simulating pressurized and boiling water reactors as well as Generation IV designs, in-house sub-channel thermal-hydraulics code SUBCHANFLOW (SCF) (Sanchez et al., 2010) is used for now.

In this paper, an internal coupling of Serpent 2 and SUBCHANFLOW is presented. It was preceded by a prototype external coupling based on Serpent 2's multi-physics interface (Daeubler et al., 2014). Thereafter, the solutions provided by Serpent 2/SUBCHANFLOW (SSS2/SCF) are verified by code-to-code benchmarking with internally coupled code MCNP5/SUBCHANFLOW (Ivanov et al., 2014) and the external coupling of TRIPOLI4 and SUBCHANFLOW (Sjenitzer, 2013; Sjenitzer et al., 2015). After the solution verification, Serpent 2/SUBCHANFLOW is employed to study a full PWR core under hot full power conditions, in particular the second exercise of the OECD/NEA and U.S. NRC PWR MOX/UO₂ core transient benchmark (Kozlowski and Downar, 2003). The obtained solutions are compared to the deterministic ones of the benchmark. The OECD/NEA and U.S. NRC PWR MOX/UO₂ core transient benchmark was selected as it includes the nuclide compositions of all fuel types loaded allowing for a Monte Carlo treatment. As the time-to-solution is considered to be important, the numerical performance of the new coupled code for the full core problem is looked at on a medium-sized parallel

computer. Finally, the hot zero power state of the BEAVRS core cycle 1 (Horelik et al., 2013) is analyzed. It represents the starting point of the process of validating the coupled solutions provided by Serpent 2/SUBCHANFLOW with measured data.

2. Internal coupling of Serpent 2 and SUBCHANFLOW

In this section, the stand-alone tools Serpent 2 and SUBCHANFLOW are introduced briefly before outlining the coupling work done.

2.1. Monte Carlo code Serpent 2

Serpent 2 (Leppänen, 2013b) is a three-dimensional continuous-energy (CE) Monte Carlo neutron transport code. A new feature that has been recently introduced into Serpent 2 is a multi-physics interface (Leppänen et al., 2012). The interface may be utilized to exchange data with thermal-hydraulics and fuel performance codes. Currently, the universal multi-physics interface comprises four types of interfaces which differ in terms of the format used for passing data between the external solver in question and Serpent. One may employ piecewise constant distributions on regular meshes (type 1), weighted averages of point-wise values (type 2), a user-defined functional dependence (type 3) or unstructured three-dimensional meshes (type 4) (Leppänen, 2012, 2014).

Utilizing the multi-physics interface implies that Serpent uses the target motion sampling method to treat the temperature dependence of the continuous-energy cross sections (Leppänen et al., 2012). TMS has been implemented in Serpent in the recent past (Viitanen and Leppänen, 2012a,b). As of now, unresolved resonances and bound-atom scattering cannot yet be treated with TMS (Viitanen and Leppänen, 2012a, 2013) severely limiting the applicability of the method for nuclear engineering applications. An alternative method to treat the temperature dependence of nuclear data in case of thermal bound-atom scattering is discussed in Section 2.5.

In its original form the TMS method relies on 0 K continuous energy cross sections and does not require a Doppler Broadening Rejection Correction (DBRC) (Viitanen and Leppänen, 2012a; Becker et al., 2009). One measure to improve the numerical performance of TMS in Serpent is to use a basis library of continuous-energy cross sections for temperatures higher than absolute zero (Viitanen and Leppänen, 2013). However, in the latter case, one has to apply DBRC again. Unfortunately, up to now, the TMS implementation in Serpent 2 is incompatible with DBRC. In this paper, basis libraries of continuous-energy cross sections for temperatures higher than absolute zero are employed for reasons of computational efficiency but no resonance upscattering is considered.

2.2. Sub-channel code SUBCHANFLOW

The sub-channel code SUBCHANFLOW solves three mixture balance equations for mass, momentum and energy in axial direction as well as an additional lateral momentum equation at sub-channel or fuel assembly level (Sanchez et al., 2010). A fully implicit method is used to solve steady-state and transient problems. Three kinds of solvers are available: a direct Gauss elimination solver for small problems, a SOR and a BiCGStab iterative solver. Because of its solution method, SUBCHANFLOW is restricted only to sub-channel upward flow.

For water material properties and state functions, the IAPWS-IF97 formulations have been adopted (Cooper et al., 2007). The heat conduction in a fuel pin is solved with a standard finite volume method. The heat transfer coefficient between fuel pin and reactor coolant is determined by using empirical correlations

depending on the heat transfer mode and flow regimes. Void fraction, pressure drop, wall friction and turbulent mixing are also calculated by means of constitutive relations.

2.3. SUBCHANFLOW as thermal-hydraulics module in Serpent 2

There are generally two options how to couple separate simulation tools into one code system: externally and internally. In an external coupling the involved codes communicate via input and output files. The execution and control of the coupled iteration is usually done by a wrapper code. Such an approach is simple as it does not require any adaption of the source of any involved tool.

In case of the external coupling of a Monte Carlo neutron transport code and thermal-hydraulics tool, the Monte Carlo geometry needs to be subdivided into a multitude of cells each corresponding to one set of TH information if the MC tool does not provide a standardized coupling interface. Investigations at KIT have shown that this process is not only error prone but also limits the application of the coupled code to small, academic problems. As mentioned in Section 2.1, Serpent 2 offers a standardized coupling interface to its users. The limitation of an external coupling to small problems does not apply to it.

Alternatively, an internal coupling approach can be utilized as done for MCNP5 and SUBCHANFLOW (Ivanov et al., 2013, 2014). In an internal coupling, the thermal-hydraulics tool is integrated into the Monte Carlo neutron transport tool as a module and information is exchanged in memory.

For the Serpent 2/SUBCHANFLOW, it was decided to couple both codes internally for two reasons. On the one hand, numerical performance would improve because large file I/O could be avoided and both tools would only have to be initialized once. Memory consumption would remain unchanged as existing structures of Serpent 2's universal multi-physics interface would be used and SUBCHANFLOW's data could be accessed directly. On the other hand, in an internal coupling the setup of a thermal-hydraulic model and its mapping to the neutron transport model would be automated reducing modeling errors. Thus, the usability would be improved.

Towards the end of an internal coupling, SUBCHANFLOW has been modularized and integrated into Serpent 2. At the moment, coupled calculations are only supported by Serpent 2/SUBCHANFLOW for k -eigenvalue criticality source calculations, not for external source or burn-up mode.

SUBCHANFLOW employs regular meshes to describe its thermal-hydraulic domain. As a consequence, the internal interface between Serpent and its module SUBCHANFLOW is based on the data structures and processing routines of the type 1 multi-physics interface already present in the Monte Carlo code.

The geometry description required by SUBCHANFLOW is prepared automatically by Serpent 2 and passed to the thermal-hydraulics module. Currently, this internal geometry pre-processor for SUBCHANFLOW is limited to reactors with square fuel lattices. However, the extension to hexagonal fuel lattices and plate type fuels is foreseen in the near future.

2.3.1. Coupled iteration algorithm

The coupled iteration algorithm of Serpent 2 and its thermal-hydraulics module SUBCHANFLOW is visualized in Fig. 1. After reading and processing the input, the already initialized internal interface between neutron transport and thermal-hydraulics is worked on. This processing of the interface includes the preparation of the thermal-hydraulic geometry description. In a next step, the module SUBCHANFLOW is initialized and executed for the first time in order to obtain an initial guess for distribution of thermal-hydraulic parameters. Serpent will apply a flat axial and radial power profile for the first thermal-hydraulics run unless the user

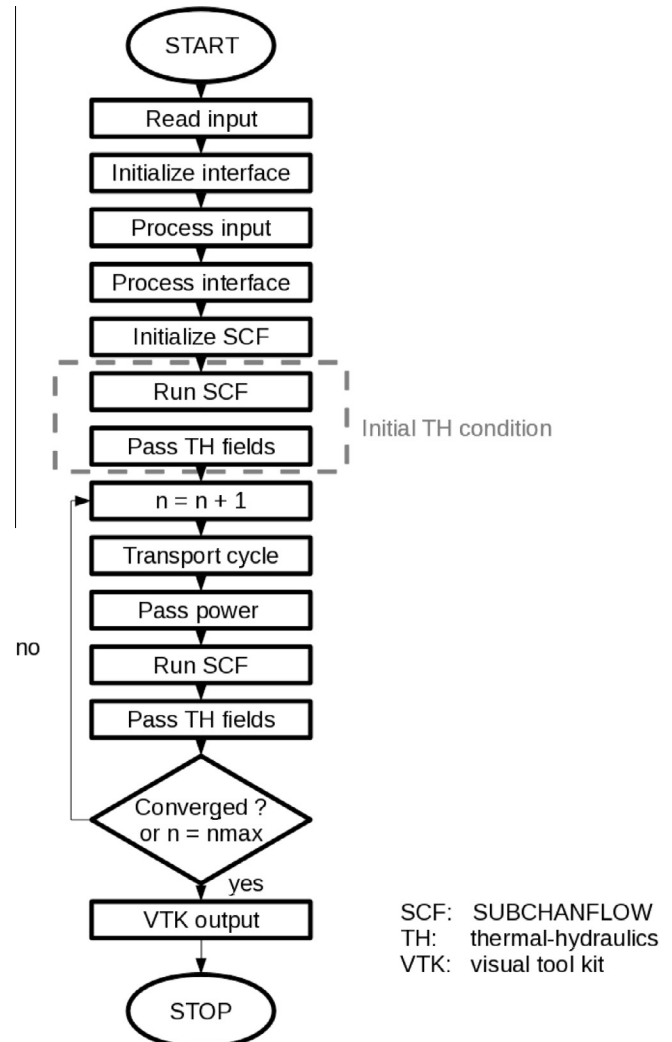


Fig. 1. Flowchart of internal coupling of Serpent 2 and SUBCHANFLOW.

explicitly specifies a profile to be used in the SUBCHANFLOW input. As using a good first guess for the power profile can save at least one coupled iteration step, it is recommended to always supply Serpent with a smart initial guess, especially for large problems like full reactor cores.

Once the initial state of the thermal-hydraulic fields has been computed, the Picard iteration is entered. A k -eigenvalue critical source calculation is performed during which heating powers are tallied. The resulting distribution is passed to SUBCHANFLOW which updates the thermal-hydraulic feedback information. While neither coupled convergence nor the maximum number of coupled iterations has been reached, the pattern is repeated. Otherwise, a Visual Tool Kit (VTK) output file is produced which allows for a detailed quantitative analysis of the results using, for example, Kitware's parallel visualization application ParaView. This VTK file contains all data fields taking part in the coupling.

The Monte Carlo tool Serpent 2 offers three different parallel modes: shared memory parallelization using the OpenMP API, distributed memory parallelization employing pure MPI (Message Passing Interface) and, finally, a hybrid parallel mode for distributed memory architectures in which MPI handles the communication between compute nodes and OpenMP is utilized for parallelization inside each node. The latter approach has a clear advantage in terms of memory consumption compared to a pure MPI implementation as Serpent duplicates its entire memory for

each MPI process. However, SUBCHANFLOW can only run in parallel on shared memory systems. As a consequence, if Serpent 2 is executed employing MPI, the thermal-hydraulics module is only run by the MPI process with rank 0. Furthermore, it is the task of the rank 0 process to collect the power tallies of all other MPI processes before executing SUBCHANFLOW and broadcasting the new thermal-hydraulic state point information to the other processes. In case of hybrid parallel execution of coupled code system, SUBCHANFLOW will run in parallel utilizing all the threads available to the master MPI process.

2.3.2. Spatial mapping

The internal coupling of Serpent 2 and SUBCHANFLOW supports channel and sub-channel thermal-hydraulics models. As part of the multi-physics interface, Serpent 2 has the capability to automatically detect fuel pin structures that completely consist of or contain materials which are affected by the interface. Moreover, it sets up power tallies in these pins. In case of a channel thermal-hydraulics model, fuel pins are grouped according to the fuel assemblies they belong to and assembly powers are computed based on tallied pin powers. If sub-channel thermal-hydraulics model is used instead, the pin powers are passed directly to the pin structures of SUBCHANFLOW. In the latter case, Serpent employs fuel pin centered feedback meshes while SUBCHANFLOW always utilizes a coolant-centered sub-channel model due to the fact that its closure relations are only validated for this case (see Fig. 2). Consequently, for square fuel lattices, radially four SUBCHANFLOW sub-channels correspond to one fuel pin in Serpent. The necessary spatial interpolation of the coolant properties is done automatically.

Even though technically possible, the radial dependence of the power production in each fuel pin is currently not modeled due to the excessively large number of neutron histories necessary to obtain statistically significant results. Nevertheless, the fuel in each fuel rod is discretized into ten radial zones to study heat transfer from the fuel to the coolant with SUBCHANFLOW. As off now, Serpent's gamma and coupled neutron-gamma transport model is still under development. As a consequence, only pure neutron transport simulations are considered in this work. Furthermore, even though the capability to tally recoil energies from the neutron

slowing down process has recently been added to Serpent 2, it is not used to keep the first version of the coupling simple. Hence, the coolant and structures like fuel rod clads are not heated directly.

Accordingly, only effective Doppler, gap and clad temperatures for each rod are provided to Serpent by the sub-channel code. Effective Doppler temperatures T_{Doppler} are determined from fuel center line $T_{f,c}$ and fuel pellet surface temperatures $T_{f,s}$ using Eq. (1).

$$T_{\text{Doppler}} = (1 - \alpha) T_{f,c} + \alpha T_{f,s} \quad (1)$$

The parameter α in the above relationship is an input parameter to be specified by the user. In the Serpent model, the temperature of the clad is set to the average of the inner cladding surface temperature $T_{\text{clad},i}$ and outer cladding surface temperature $T_{\text{clad},o}$. Correspondingly, the temperature of the gas in the gap is assumed to be the average of inner cladding surface temperature $T_{\text{clad},i}$ and fuel pellet surface temperature $T_{f,s}$.

All thermo-mechanical effects like thermal expansion are neglected. Moreover, as the current version of the coupling focuses on LWR, the temperature dependence of the densities of all materials except the coolant is assumed to marginally influence the overall result and is, resultantly, not accounted for.

2.3.3. Convergence checking

To check the convergence of the coupled fields, the relative l^2 -norm or Euclidean norm of Doppler temperature and moderator density distribution are computed as demonstrated in Eq. (2). Vector X describes the solution field of Doppler temperature or moderator density, n denotes the current iteration step and $n - 1$ the previous step.

$$\frac{\Delta X}{X} = \frac{\|X^n - X^{n-1}\|_{l^2}}{\|X^n\|_{l^2}} \leq \epsilon_X \quad (2)$$

The convergence criterion ϵ_X in Eq. (2) is defined by the user. The l^2 -norm or Euclidean norm is preferred by the authors over the commonly applied maximum or ∞ -norm as it includes information on all off the solution space and not just a single point of that space.

Besides checking the convergence of fuel temperature and moderator density, the relative change in eigenvalue is monitored according to Eq. (3), again employing a user-specified convergence criterion ϵ_k .

$$\Delta k_{\text{eff}} \leq \epsilon_k \quad (3)$$

It is generally understood that the convergence of coupled Monte Carlo thermal-hydraulic code systems is limited by the maximum statistical uncertainty of the Monte Carlo power tallies. As a consequence, it is beneficial to undertake efforts to reduce this maximum uncertainty by applying global variance reduction techniques. While for small models such as single LWR fuel assemblies a decent convergence of the coupled solution may still be achieved without global variance reduction techniques, these prove to be essential for more realistic, larger models like an entire LWR active reactor core.

In 2010, the Uniform-Fission-Site (UFS) method has been implemented in Serpent by VTT, it is similar to the one used by Kelly et al. (2012). With this method one tries to increase the number of fission source points in regions where the fission powers is low, thus, decreasing statistical uncertainties in these regions. In Serpent 2, a regular Cartesian mesh is superimposed on the geometry. In the cells of this mesh, either collision points, neutron flux or fissions are tallied during the inactive cycles of a calculation. The collected results are used to adjust the number of fission neutrons being emitted in the active cycles.

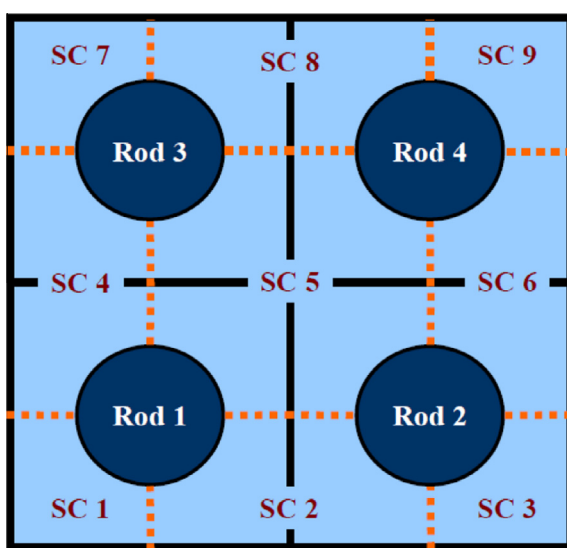


Fig. 2. Exemplary comparison of Serpent's multi-physics interface and SUBCHANFLOW regular meshes for a 2×2 fuel pin cluster: multi-physics interface mesh cell boundaries (black) and sub-channel boundaries in the T/H model (orange), taken from Gomez-Torres et al. (2012a). (For interpretation of the references to color in this figure legend, the reader is referred to the web version of this article.)

In this work, the regular mesh of the UFS method is chosen to be identical to the feedback meshes used by the internal interface. Furthermore, collision points are scored during the inactive cycles of a criticality source simulation. However, the number of inactive neutron histories has to be sufficiently large to provide good statistics for the UFS method.

With a setup of the Picard iteration as it is done in Serpent 2/SUBCHANFLOW, it is crucial that the power distribution tallied is based on a converged fission source. Brown (2006) proposed to use the Shannon entropy to measure the convergence of the fission source distribution. Serpent 2 has the capability to compute the x -, y - and z -components of the Shannon entropy. If necessary, the Shannon entropy can also be evaluated on a mesh superimposed on the geometry. The latter option is especially useful for large models to detect possible unphysical asymmetries in the neutron flux solution. Consequently, it is employed to assess the convergence of the fission source for the coupled code developed.

Furthermore, a method to improve the convergence of the fission source as well as the symmetry of the neutron flux solution is discussed in Section 2.4, the Wielandt shift.

2.3.4. Implemented under-relaxation scheme

Past research on deterministic reactor simulators as well as coupled Monte Carlo thermal-hydraulic code systems has emphasized the usefulness of under-relaxation schemes to achieve both a faster and a smoother coupled convergence. Recently, Dufek and Hoogenboom (2014) have derived a stable relaxation scheme for coupled Monte Carlo neutron transport and thermal-hydraulics simulations. In their scheme, the relaxed normalized neutron flux ϕ^n obtained in iteration step n is given in terms of the unrelaxed normalized neutron flux $\tilde{\phi}$ solutions of all steps (see Eq. (4)).

$$\phi^n = \frac{1}{n} \sum_{i=1}^n \tilde{\phi}^i \quad (4)$$

Fortunately, Eq. (4) can be rewritten in a recursion form as shown in Eq. (5). The second form is preferable. Only the old relaxed flux distribution needs to be saved while the memory demand of the former version increases linearly with the iteration index n .

$$\phi^n = \left(1 - \frac{1}{n}\right) \phi^{n-1} + \frac{1}{n} \tilde{\phi}^n \quad (5)$$

From Eq. (4) the benefit of this relaxation scheme for a coupled Monte Carlo thermal-hydraulics calculation becomes clear. Combining the flux solutions of all previous iteration steps leads to a reduction of the statistical errors in the relaxed fluxes. However, in Serpent 2/SUBCHANFLOW, it is actually applied to power distributions obtained from neutron fluxes instead of the neutron fluxes themselves.

2.4. Wielandt shift implementation

A full PWR core is a loosely coupled system since the mean free path of neutrons of all energies is significantly smaller than the spatial extend of the core. To obtain a well converged Monte Carlo neutron transport solution one would traditionally pre-compute a converged fission source file and would then run a second calculation based on the pre-determined source distribution. Alternatively, one could try to pre-condition the problem to improve convergence behavior. One such method, which is widely used in low-order deterministic reactor simulators, is the Wielandt shift.

The static neutron transport equation can be written in the following operator form

$$\mathbf{M}\phi = \frac{1}{k_{\text{eff}}} \mathbf{F}\phi = \lambda \mathbf{F}\phi \quad (6)$$

with $\mathbf{M} = \mathbf{D} + \mathbf{T} + \mathbf{S}$ where \mathbf{D} is the streaming operator, \mathbf{T} the absorption operator and \mathbf{S} the scattering operator. Furthermore, \mathbf{F} is the fission operator. The Wielandt method relies on modifying the transport operator \mathbf{M} . A fixed fission source is subtracted from both sides of Eq. (6) yielding Eq. (7). As can directly be seen from Eq. (7), the eigenfunctions of the modified neutron transport equation are identical to those of the original equation. The eigenvalues, however, are not.

$$(\mathbf{M} - \lambda_{\text{shift}} \mathbf{F})\phi = (\lambda - \lambda_{\text{shift}})\mathbf{F}\phi \quad (7)$$

The change in eigenvalue spectrum leads to an improved convergence behavior of the power iteration if $\lambda > \lambda_{\text{shift}} = 1/k_{\text{shift}}$ (Brown, 2007).

The Wielandt shift in Serpent 2 was tested using the OECD/NEA and U.S. NRC PWR MOX/UO₂ core transient benchmark (Kozlowski and Downar, 2003) 2D HZP state defined in the following. The loading pattern for a quarter of the Westinghouse 4-loop PWR core in question is shown in Fig. 3. The colors in the layout indicate different fuel assembly batches. Green refers to the first, yellow to the second and red to the third batch. Both UOX (U) and MOX (M) fuel assemblies of different enrichments are loaded in this cycle. Furthermore, positions of control and shutdown banks as well as fuel assembly burn-ups in GWd/tU are indicated. A 2D simulation with fixed thermal-hydraulic conditions was carried out which are listed in Table 1. For the neutron transport calculation all control and shutdown banks are considered to be fully withdrawn. ENDF/B VII.0 evaluated nuclear data is employed.

Serpent 2 simulated $4 \cdot 10^6$ neutrons per cycle. Based on the Shannon entropy distribution evaluated on a 5×5 mesh superimposed on the geometry, it was decided to employ 100 inactive cycles. To tally power, 600 active cycles followed.

The fission source convergence was assessed for different choices of k_{shift} . Using the average fission chain length as defined by Brown (2007), the number of active cycles was adjusted to yield approximately the same number of collisions simulated in total. To examine the influence of Wielandt's method on local reaction rates, assembly powers were tallied in all Serpent 2 runs. The figure of merit given in Eq. (8) is employed to evaluate that influence. Here, N is the number of tally bins, T the average wall clock time and σ_i standard deviation of each tally bin estimated based on 10 replica runs.

$$FOM = \frac{N}{T \sum_i \sigma_i^2} \quad (8)$$

The results of the implementation testing are listed in Table 2. Utilizing the modified transport operator, Serpent 2 reproduces the reference eigenvalue obtained with an unchanged transport operator within the statistical uncertainty. The number of cycles to converge the fission source and the number of active cycles steadily decreases with decreasing difference between shift eigenvalue and true eigenvalue of the system. This is due to the increasing length of the fission chains simulated in one cycle. Correspondingly, the unwanted inter-cycle correlation in stochastic neutron transport process is reduced. At the same time, an improvement of the FOM for the assembly power tally is observed.

Ivanov et al. (2014) reported that Wielandt's method leads to more symmetric tallies since it diminishes the inter-cycle correlations in a criticality source calculation. The PWR core studied in the OECD/NEA and U.S. NRC PWR MOX/UO₂ core transient benchmark has eight fold symmetry. As a result, it is a very good test case for tally symmetry. Employing the unchanged transport operator, Serpent 2's assembly power tally exhibited a maximal asymmetry of 2.41% on average. Running the neutron transport

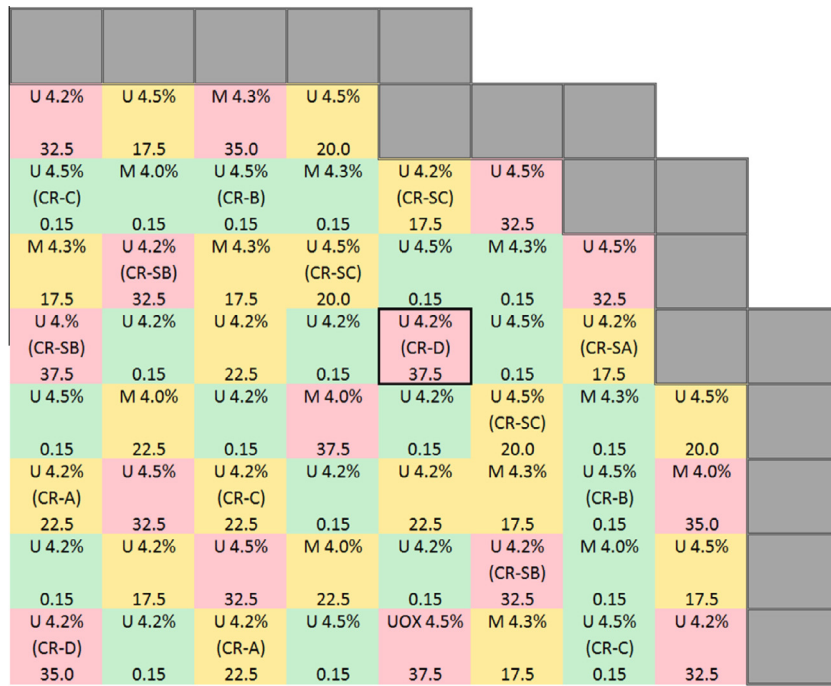


Fig. 3. Layout of a quarter of the PWR core of the OECD/NEA and U.S. NRC PWR MOX/UF₆ core transient benchmark.

Table 1

Fixed thermal-hydraulic conditions for 2D cases of the OECD/NEA and U.S. NRC PWR MOX/UF₆ core transient benchmark.

Parameter	Value
Core power	1 W
Core temperature	560 K
Boron concentration	1000 ppm

Table 2

Comparison of results obtained for different eigenvalue shifts.

Shift eigenvalue	SSS2 k_{eff}	Inactive cycles	Active cycles	FOM
∞	1.05862 ± 0.00005	100	600	1.47
1.30	1.05863 ± 0.00004	30	200	2.49
1.16	1.05863 ± 0.00004	14	140	3.07
1.10	1.05862 ± 0.00003	7	60	6.81

with a shift eigenvalue of 1.10 lead to a reduction of this asymmetry to 0.77% on average.

The neutron transport equation solved by deterministic methods describes the behavior of the mean neutron flux averaged over an infinite number of single particle histories. This mean neutron flux always exhibits the symmetry of the underlying reactor core geometry. Monte Carlo methods, however, can only simulate a limited number of neutron histories. In the latter case, the physical effect of particle clustering becomes visible. The neutron flux solution no longer necessarily has the symmetry of the reactor core loading. For a detailed discussion of particle clustering please refer to Dumonteil et al. (2014). Since the authors want to use Monte Carlo neutron transport to estimate the mean neutron flux obtainable with deterministic solutions, handling the tally asymmetry is crucial for large problems such as full PWR core even though it reflects a physical reality. In order to estimate this mean neutron flux in a reasonable amount of time, the Wielandt shift is an essential feature of the coupled code system Serpent 2/SUBCHANFLOW. However, the increasing length of the fission chains in one cycle leads to a steep increase in computation time. The Serpent 2

solution not using Wielandt shift (Table 2) consumed 272 CPUh. The one employing a shift of 1.10 needed 715 CPUh on a Intel Xeon E5-2670 processor. One might argue that running the conventional Serpent 2 for 715 CPUh should also significantly improve the symmetry of the tallies. In fact, the symmetry improves by roughly 40% compared to the run taking 272 CPUh. Using Wielandt's method, the tally symmetry is, however, improved by almost 70% compared to the reference run.

Unfortunately, the computational burden of the Wielandt shift limits the authors to employing it to 2D cases and for producing converged fission source files for 3D coupled simulations. To finish a full 3D HFP coupled simulation employing Wielandt's method in a reasonable amount of time requires larger computational resources than available to the authors. The latter runs still employ the Uniform Fission Site method to reduce global variance.

2.5. Stochastic mixing fallback for TMS method

The target motion sampling (TMS) method is a stochastic method to account for the effect of thermal motion in a Monte Carlo neutron transport calculation. This technique allows to perform on-the-fly Doppler broadening of incident neutron free atom cross sections. It is based on sampling the target velocities from a Maxwell-Boltzmann distribution at the collision sites. Followed by a transformation into the target-frame to solve the reaction physics for a given temperature. TMS cannot be used for thermal bound-atom scattering since the chemically bound target atoms do not have velocities that are distributed according to Maxwell-Boltzmann in thermal energy range. A detailed description of TMS can be found in Viitanen and Leppänen (2012a,b, 2013).

Alternative on-the-fly schemes for treating the temperature dependence of free atom cross sections in the resolved range are available or being developed in MCNP6 (Martin et al., 2013) and OpenMC (Forget et al., 2014). However, most other coupled Monte Carlo thermal-hydraulics solutions adapt stochastic mixing or pseudo materials as a practical approach to treat the temperature dependence of nuclear data (Bernnat et al., 2012; Trumbull and Fieno, 2012; Vazquez et al., 2012; Ivanov et al., 2014).

Stochastic mixing is beneficial compared to a brute force temperature treatment in Monte Carlo neutron transport. In such a brute force treatment, one would pre-generate nuclear data at very small temperature intervals, say 1 K, and load the entire library into memory for usage during the transport cycle. This approach consumes an enormous amount of memory which the pseudo material approach is able to reduce by allowing for larger temperature spacing of the nuclear data. While the former solutions apply stochastic mixing to tackle the problem of thermal motion as a whole, the pseudo material approach is only to be applied in Serpent 2/SUBCHANFLOW for the nuclides affected by thermal bound-atom scattering.

In the pseudo material approach, each nuclide in material is represented by two sets of nuclear data. The sets of data are evaluated at temperatures T_{low} and T_{high} which enclose the actual temperature T of the material in question. In the case of linear mixing, the fraction of use of the nuclear data set with the lower temperature is obtained from Eq. (9).

$$f = \frac{T_{\text{high}} - T}{T_{\text{high}} - T_{\text{low}}} \quad (9)$$

Accordingly, the fraction of the cross sections evaluated at the higher temperature T_{high} is $1 - f$. The stochastic mixing approach is not an interpolation in the classical sense. No nuclear data is ever generated at temperature T . The method relies on the stochastic nature of the neutron transport process. For a sufficiently large number of neutron histories, the above approach is equivalent to using the below expression for the cross sections

$$\Sigma(T) = f \Sigma_{\text{low}}(T_{\text{low}}) + (1 - f) \Sigma_{\text{high}}(T_{\text{high}}) \quad (10)$$

which is effectively a linear interpolation.

One of the first to propose the stochastic mixing approach was van der Marck et al. (2005) who used a square root mixing coefficient instead of the linear one presented here in Eq. (9). Only slightly later, Trumbull assessed different interpolation techniques for free atom cross sections at different temperatures (Trumbull, 2006). He showed that for the linear interpolation of free atom cross sections (see Eq. (10)) the linear interpolation coefficient is more accurate than the square root one in all his test cases. Hence, in Serpent 2/SUBCHANFLOW a linear mixing coefficient is utilized.

For stochastic mixing as interpolation technique, the maximum acceptable temperature spacing of nuclear data sets needs to be assessed. Trumbull (2006) assessed this question for free atom continuous-energy cross sections. He defined relative differences of <0.1% between interpolated and reference cross section in every point to be acceptable. He found that for nuclides with a complex resonance structure even the smallest applied data set spacing of 28 K could not satisfy his criterion. For other nuclides, however, temperature spacings of up to 111 K produced acceptable results.

Most moderator materials in thermal reactors do not exhibit complex resonance structures in their free atom cross sections. Thus, based on Trumbull's findings one expects that large temperature spacings of the scattering nuclides for the stochastic mixing fall back algorithm are acceptable. To test this hypothesis, the verification model briefly introduced in the following is employed.

An infinite lattice of 3.65755 m long fresh 4.2 wt% enriched uranium oxide (UOX) fuel pins is studied employing ENDF/B VII.0 evaluated nuclear data. The pin is surrounded by light water as coolant forming a square pin cell with 1.26 cm side length. The remaining geometry and material details of the model are summarized in Table 3.

The water surrounding the UOX fuel pin was divided into two axial zones of equal height. In the first zone, the temperature of

Table 3

Geometry and material details of stochastic mixing fall back verification model.

Quantity	Value
Pellet radius	0.3951 cm
Inner clad radius	0.4010 cm
Outer clad radius	0.4583 cm
Fuel material	UOX 4.2 wt%
Gap material	Oxygen
Clad material	Zircaloy 4
Coolant material	Water
UOX density	10.242 g/cm ³
Gas density	10 ⁻³ g/cm ³
Clad density	6.5047 g/cm ³
Coolant density	0.75311 g/cm ³

the water was set to be 500 K and in the second one 600 K. The temperature of the fuel pellet was assumed to be 900 K, clad and gas gap were kept at 600 K throughout the model.

The two water zones were modeled using two separate approaches. In the reference model, the cell containing the water was subdivided axially. For each of the two new cells a water material at 500 K and 600 K, respectively were defined.

For the fall back test model, the $S(\alpha, \beta)$ scattering tables for 500 K and 600 K were removed from Serpent 2's ENDF/B VII.0 library forcing the code to apply pseudo material mixing. As the ENDF/B VII.0 $S(\alpha, \beta)$ evaluations are provided in 50 K intervals in that temperature range, the interpolation for both water zones is done over an 100 K interval. To characterize the neutron behavior in all materials of the model spectra are tallied in the SCALE 238 energy group structure (ORNL, 2011) which is well suited for analyzing light water reactors.

In order to ensure sufficient statistics for the fine energy group structure tallies, $2 \cdot 10^6$ neutrons were simulated per cycle. 600 active cycles followed 20 inactive cycles. Based on the Shannon entropy, the latter was enough to converge the fission source.

Without loosing any generality, only the neutron spectrum in the first water zone is shown in Fig. 4 and analyzed in the following. In the thermal energy range, relative differences as high as 2.25% are observed (energies below 10^{-9} MeV are disregarded because of too low statistics). While the stochastic mixing of free atom cross sections for hydrogen over the 100 K temperature interval leads to no detectable change in simulation results, the introduction of $S(\alpha, \beta)$ in the process does.

Besides cross sections the $S(\alpha, \beta)$ scattering data tables include distributions for the out-going energies and angles of the interacting neutrons. The authors found that the linear interpolation like stochastic mixing leads to good results for cross sections and out-going neutron energy distributions. However, the angular distribution needs to be handled with an inverse interpolation scheme. For large temperature spacing of the scattering nuclides employed by Serpent 2 the effect of using a linear instead of a inverse interpolation on the angles becomes large. As a result, one would like to increase the number of thermal scattering data files evaluated at unique temperatures.

Serpent 2 employs $S(\alpha, \beta)$ tables prepared by the LEAPR-THERMR-ACER sequence of the nuclear data processing tool NJOY. The module LEAPR requires frequency spectra $\rho(\omega)$ of the scattering nucleus at each temperature a $S(\alpha, \beta)$ scattering law is to be generated. Thus, unfortunately, the temperatures at which thermal scattering data tables for Serpent can be generated are defined by the temperatures for which $\rho(\omega)$ of the scattering nucleus is available. For both ENDF/B VII.0 and JEFF 3.1.1, 9 and 11 temperature points are available spanning roughly 300 K to 800 K for ENDF/B and 300 K to 1000 K for JEFF. Mattes and

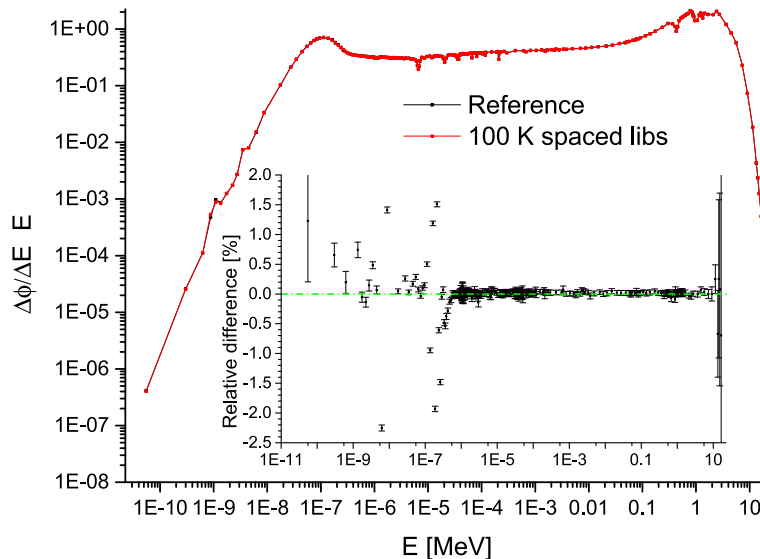


Fig. 4. Comparison of neutron spectra in first water zone predicted with and without stochastic mixing fall back using 100 K spaced libraries.

Keinert (2005) provide an interpolation scheme for $\rho(\omega)$ in their report. It was tested whether interpolating the frequency spectrum and then running LEAPR-THERMR-ACER is more accurate than interpolating $S(\alpha, \beta)$ tables for given frequency spectra. In all our test cases no clear advantage of interpolating the frequency spectra with the method of Mattes and Keinert was observed. Consequently, at the moment the option of choice to improve the accuracy of the stochastic mixing with $S(\alpha, \beta)$ scattering laws involved is to interpolate cross sections and out-going energies linearly and angles inversely as this proved to produce the most accurate results. For Serpent 2/SUBCHANFLOW this interpolation is not done on-the-fly but interpolated thermal scattering data is prepared.

Nevertheless, the question of how large a spacing of interpolated scattering data tables could be remains to be answered. To this end, the infinite lattice of finite height UOX fuel pins is studied once more. Like for the first test presented in this section, Serpent 2 is forced to interpolate as the thermal scattering data sets belonging to the exact solution have been removed from its library. By adding newly generated externally interpolated $S(\alpha, \beta)$ tables to the library, Serpent uses a 20 K, 10 K and 5 K temperature interval in the stochastic mixing method. It is the aim of the following test to determine the remaining errors relative to the reference solution.

Figs. 5–7 depict the neutron spectra in the first water zone and their relative difference to the reference solution. Going from a 100 K to a 20 K temperature increment of the thermal scattering data already significantly reduces the observed errors in the neutron flux from maximum of 2.25% to 0.65% for thermal energies above 10^{-9} MeV. The maximal difference between the stochastic mixing and the reference solution are basically the same for 10 K and 5 K spaced data sets. However, the mean square error 0.105% of the 5 K case is significantly lower than 0.163% for the 10 K case. If memory consumption does not prohibit the usage of 5 K spaced thermal scattering data, it is the best choice in terms of accuracy.

3. Solution verification for Serpent 2/SUBCHANFLOW

In the two selected verification cases presented in this paper, Serpent 2/SUBCHANFLOW was benchmarked with an external coupling of TRIPOLI4 and SUBCHANFLOW as well as an internally coupled MCNP5/SUBCHANFLOW. It was decided to only utilize Monte

Carlo neutron transport based reference solutions to exclude differences introduced by different neutron transport methods.

3.1. Channel thermal-hydraulics

The first case studied to verify the Serpent 2/SUBCHANFLOW solution employing a channel level thermal-hydraulics model is 3×3 PWR fuel assembly cluster surrounded by one row of water reflectors (see Fig. 8). This case was defined as part of the NURISP boron dilution benchmark. Both the $17 \times 17 - 25$ mixed oxide (MOX) and $17 \times 17 - 25$ UOX fuel assemblies have no burn-up. Their initial enrichment can be read from Fig. 8. The geometry and material definition of the fuel assemblies in the NURISP boron dilution benchmark were taken from the OECD/NEA and U.S. NRC PWR MOX/UO₂ core transient benchmark (Kozlowski and Downar, 2003). A summary of the HFP operating conditions for this minicore are given in Table 4.

For this reflected 3×3 fuel assembly cluster the parameter α in the expression to evaluate the effective Doppler temperature (see Eq. (1)) was set to 5/9 to be consistent with the given TRIPOLI4/SUBCHANFLOW solution.

Both Serpent 2 and TRIPOLI4 utilize JEFF 3.1.1 evaluated nuclear data. For Serpent 2's stochastic mixing fall back for TMS a 5 K spacing of $S(\alpha, \beta)$ scattering data sets was chosen. TRIPOLI4 employed a 50 K spaced cross section library for its pseudo materials. Like Serpent 2, it employs linear mixing coefficients.

In the Serpent 2/SUBCHANFLOW model, there are 20 axial layers in the thermal-hydraulic feedback mesh. In TRIPOLI4, the geometry was divided into 17 axial layers for the external coupling.

Serpent 2/SUBCHANFLOW used 400 inactive and 1200 active cycles of $5 \cdot 10^6$ neutrons each per coupled iteration. Setting Doppler temperature and moderator density coupled convergence targets to 1%, Serpent 2/SUBCHANFLOW converged after only 4 iterations.

A comparison of the minicore eigenvalues predicted by Serpent 2/SUBCHANFLOW and TRIPOLI4/SUBCHANFLOW is given in Table 5. As can be seen from this table, TRIPOLI4/SUBCHANFLOW solution settled for lower statistics. The difference in eigenvalue of 36 ± 43 pcm is not statistically significant.

Looking at the normalized, axially integrated assembly powers as predicted by both coupled codes in Fig. 9, a good agreement is

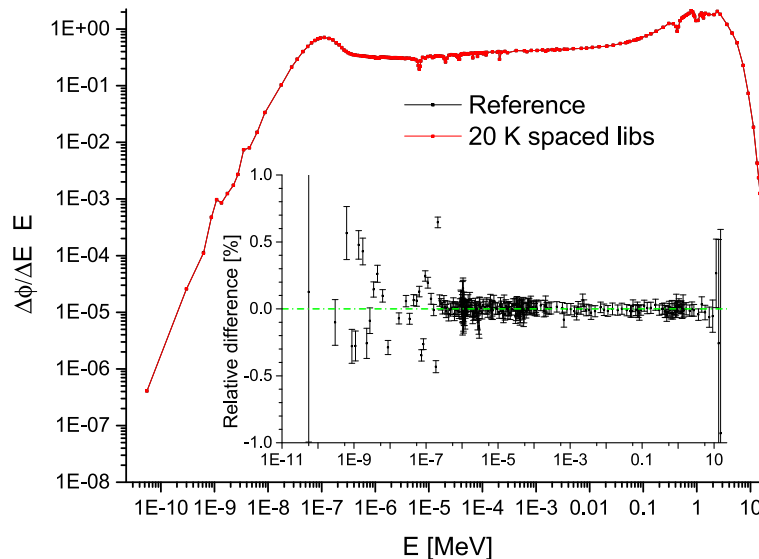


Fig. 5. Comparison of neutron spectra in first water zone predicted with and without stochastic mixing fall back using 20 K spaced libraries.

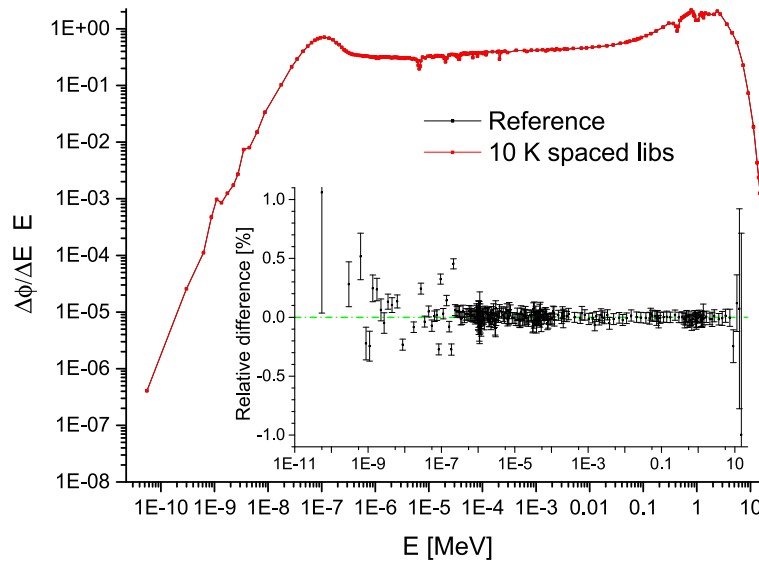


Fig. 6. Comparison of neutron spectra in first water zone predicted with and without stochastic mixing fall back using 10 K spaced libraries.

observed. However, due to the relatively small number of neutron histories the TRIPOLI4 flux solution is not perfectly symmetric even though the underlying geometry is. The maximum relative difference between Serpent 2/SUBCHANFLOW and TRIPOLI4/SUBCHANFLOW results is 1.6%. It is statistically significant as the corresponding uncertainties in the power tally are below 0.5% in the last iteration of both coupled solutions. In case of Serpent 2/SUBCHANFLOW, the statistical uncertainties of the power tallies in the last iteration can only be an estimate of the true uncertainty in the power distributions.

Moving from the axially integrated power distribution to the axial power distribution of each individual assembly, the deviations between both coupled solutions are more pronounced. Without a loss of generality, the following discussion is limited to the central fuel assembly of the minicore, assembly number 5 (see Fig. 8). The axial power profile of this fuel assembly as predicted by Serpent 2/SUBCHANFLOW and TRIPOLI4/SUBCHANFLOW is contrasted in Fig. 10. Generally, the both profiles have a very similar shape. The profile predicted by Serpent 2/SUBCHANFLOW is slightly more shifted to the lower half of assembly number 5.

In order to be able to quantitatively compare both simulation results, Serpent 2/SUBCHANFLOW powers were histopolated to the lower number of axial layers employed by the other solution. At the bottom of this particular fuel assembly local differences in power as high as 30% of the Serpent 2/SUBCHANFLOW solution are observed. In most of the axial bins, however, the relative differences between both solution are well below 10%. These differences are significant as statistical uncertainty in power was below 1.1% everywhere for TRIPOLI4 and below 0.2% for Serpent 2. The axial distribution of the coolant temperature in the channel belonging to assembly 5 is depicted in Fig. 11. As the largest deviations in power between both coupled solutions appear in low power regions, the coolant temperature profiles match very well.

The question how to estimate the statistical uncertainty of the thermal-hydraulic data fields arises trying to evaluate the significance of the found deviations. Unfortunately, up to now no method to determine the true statistical uncertainty of the thermal-hydraulic state point information or the neutron flux during a single calculation exists. The only option is to perform a sufficiently large number of replica runs, i.e. repeating the coupled simulation with

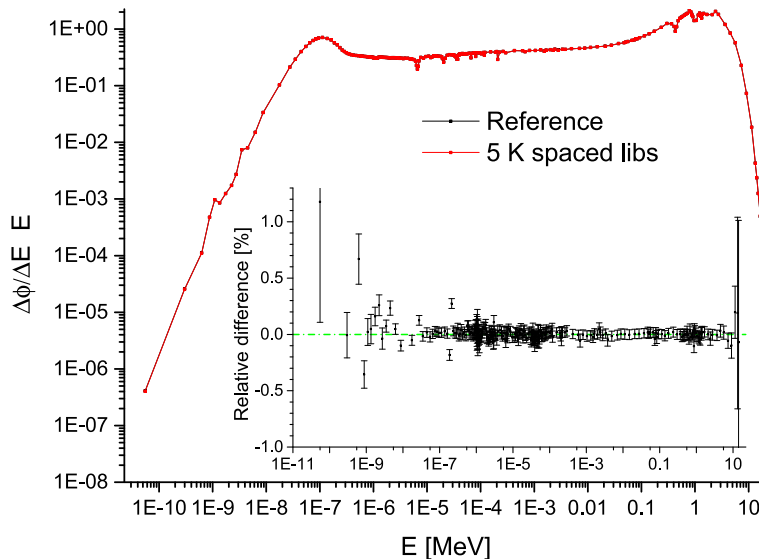


Fig. 7. Comparison of neutron spectra in first water zone predicted with and without stochastic mixing fall back using 5 K spaced libraries.

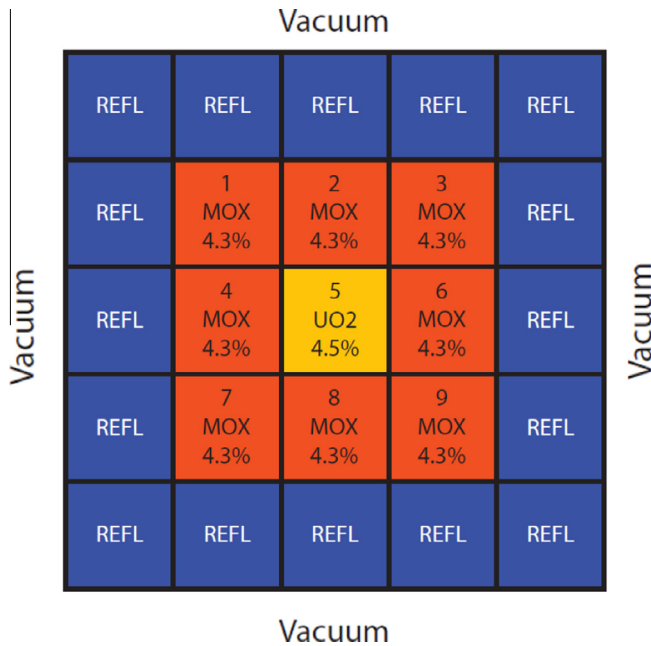


Fig. 8. Layout of the 3×3 PWR fuel assembly reflected minicore, taken from Sjenitzer (2013).

Table 4

HFP operating conditions of reflected 3×3 minicore of NURISP boron dilution benchmark.

Quantity	Value
Power	100 MW
Core mass flow rate	739.08 kg/s
Outlet pressure	15.4 MPa
Coolant inlet temperature	560 K
Boron concentration	200 ppm

different starting values of the seed of the random number generator. Thereafter, one needs to analyze the spread of the results of the replica runs with statistical methods in order to approximate mean and standard deviation.

Table 5
Comparison of minicore HFP k -eigenvalues.

Coupled code	k_{eff}
TRIPOLI4/SCF	1.01861 ± 0.00043
SSS2/SCF	1.01825 ± 0.00002

Since no statistical uncertainty information is available for the TRIPOLI4/SUBCHANFLOW solution and performing a sufficiently large number of replica runs corresponds to using a large amount of computational resources, the comparison of thermal-hydraulic fields is only done qualitatively for this case.

The versions of SUBCHANFLOW used together with TRIPOLI4 and Serpent 2 utilize the same water/steam tables. As a result, no new insight is to be gained from comparing moderator density profiles for the central assembly. Instead, the axial profile of the effective Doppler temperatures determined by both coupled codes was analyzed. The local differences between both solutions exhibit the same behavior as the differences in power.

Since Serpent 2 and TRIPOLI4 receive their feedback information from two versions of the same thermal-hydraulics tool and it has been verified that both thermal-hydraulic models were comparable in terms of constituent relations and options employed, the observed deviations can be attributed to differences in the neutronics solution.

Both Monte Carlo codes used data from the JEFF 3.1.1 nuclear data evaluation. However, they did not utilize the same library. Serpent employed an ACE library built from JEFF 3.1.1 nuclear data while TRIPOLI used the ENDF formatted JEFF 3.1.1 information directly. More importantly, the methodology for treating the temperature dependence of nuclear data was different between both solutions. While the TMS method employed by Serpent 2 is in principle as accurate as the employed ACE cross section files, the pseudo material mixing approach used by TRIPOLI4 is not. Only a slight approximation is introduced in TMS through the cut-off condition of the infinite tail of the Maxwell-Boltzmann distribution.

Last but not least, TRIPOLI4 applied a resonance upscattering correction while Serpent 2 did not as it is incompatible with TMS at this point in time.

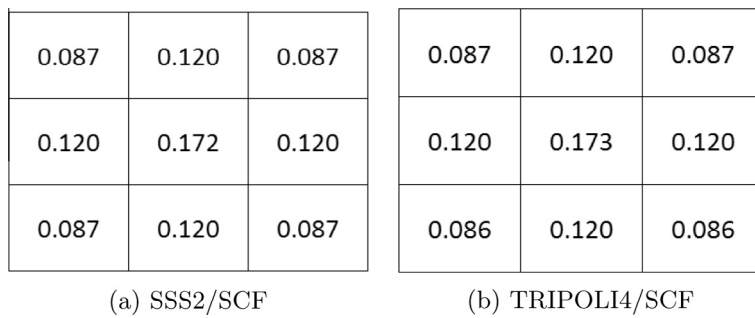


Fig. 9. Radial power profiles of 3×3 reflected minicore as predicted by Serpent 2/SUBCHANFLOW and TRIPOLI4/SUBCHANFLOW.

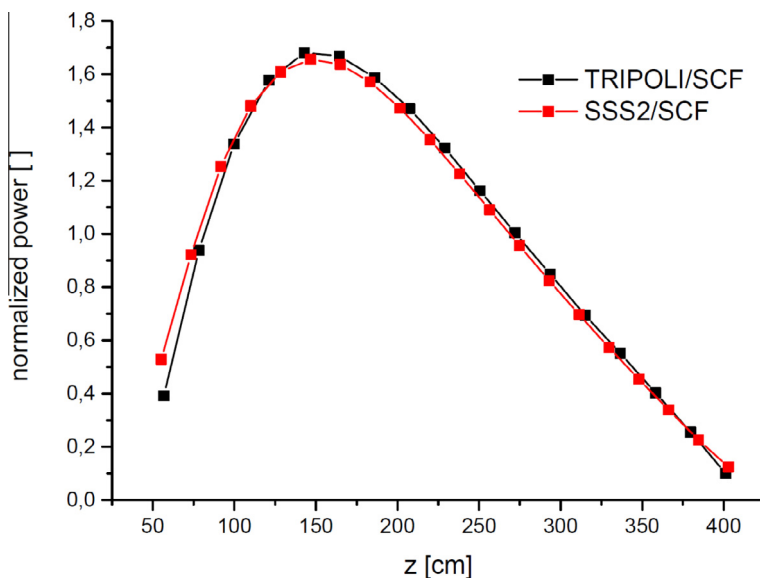


Fig. 10. Comparison of normalized power profile in central fuel assembly of the minicore.

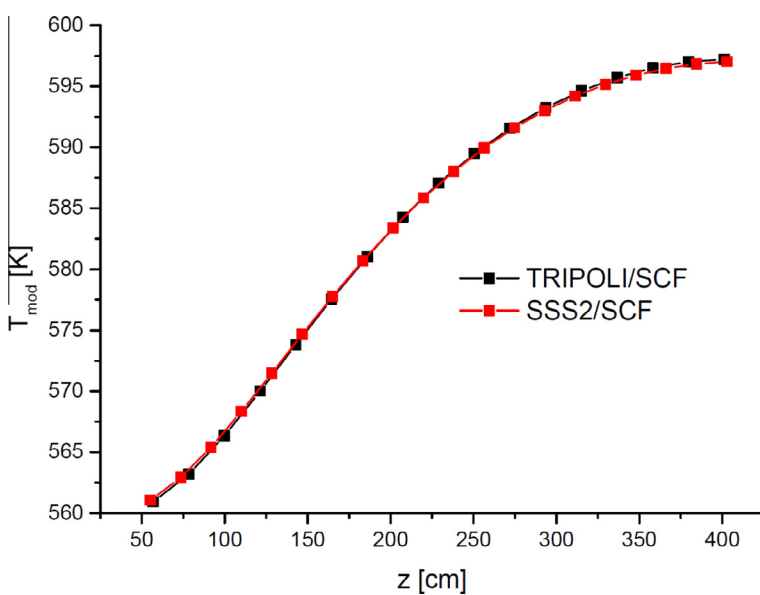


Fig. 11. Comparison of moderator temperature in Kelvin in central fuel assembly of the minicore.

3.2. Sub-channel thermal-hydraulics

The second verification case analyzed is also a 3×3 PWR fuel assembly cluster shown in Fig. 12. This case has been developed in the framework of the High Performance Monte Carlo Project (HPCM) which is performed under the seventh EURATOM Framework Programme for nuclear research and training activities. Like for the previous channel level thermal-hydraulics case, the $17 \times 17 - 25$ MOX and $17 \times 17 - 25$ UOX assemblies the minicore consists of are fresh. Moreover, their geometry and material specification has been taken from the OECD/NEA and U.S. NRC PWR MOX/UO₂ core transient benchmark (Kozlowski and Downar, 2003). In the UOX assembly, however, the integral burnable absorber rods (IFBA) are replaced with unpoisoned fuel pins. The hot full power operating conditions for this case are given in Table 6.

For this verification case employing a sub-channel thermal-hydraulics model, Serpent 2/SUBCHANFLOW is benchmarked against an internal coupling of MCNP5 and SUBCHANFLOW (Ivanov et al., 2014). Both Serpent 2 and MCNP5 employed JEFF 3.1.1 evaluated nuclear data. Like for the channel thermal-hydraulics case, 5 K spaced $S(\alpha, \beta)$ scattering data sets were included in Serpent 2's library. MCNP5 utilized a 50 K spaced cross section library for its pseudo material approach to treat temperature dependence of nuclear cross sections. Like in Serpent 2, linear mixing coefficients are used. The $S(\alpha, \beta)$ tables, however, are interpolated on-the-fly using an advanced interpolation scheme.

Both coupled codes model the axial dependence of the thermal-hydraulic state point information in 20 axial layers. The coefficient α for calculating the effective Doppler temperatures according to Eq. (1) is set to 0.7.

Serpent 2/SUBCHANFLOW tracked a total of $6.0 \cdot 10^9$ neutrons per coupled iteration. Setting Doppler temperature and moderator density coupled convergence targets to 0.05%, Serpent 2/SUBCHANFLOW converged after only 8 iterations. MCNP5/SUBCHANFLOW simulated $3.0 \cdot 10^8$ neutron histories per coupled iteration step. It required 33 iterations for the maximum change in effective Doppler temperature to fall below 0.05%.

The effective multiplication factor of the 3×3 fuel assembly cluster predicted by both coupled codes is listed in Table 7. A 106 ± 4.1 pcm difference is observed. In the following the thermal-hydraulic parameter fields are analyzed to identify factors contributing to this deviation. Unfortunately, a pin power distribution is not available for the MCNP5/SUBCHANFLOW solution.

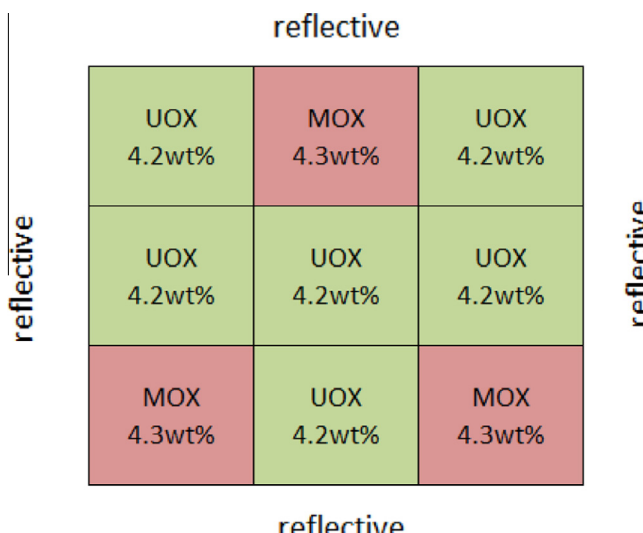


Fig. 12. Layout of the 3×3 PWR fuel assembly cluster as defined in HPMC project.

Table 6

HFP operating conditions of HPMC project 3×3 fuel assembly cluster benchmark.

Quantity	Value
Power	166.24 MW
Core mass flow rate	739.09 kg/s
Outlet pressure	15.45 MPa
Coolant inlet temperature	560 K
Boron concentration	1200 ppm

Table 7

Comparison of HPMC 3×3 fuel assembly cluster HFP k -eigenvalues.

Coupled code	k_{eff}
MCNP5/SCF	1.22298 ± 0.00004
SSS2/SCF	1.22192 ± 0.00001

Thus, the analysis focuses on effective Doppler and moderator temperatures. As both versions of SUBCHANFLOW employed by each solution utilize the same water/steam tables, it is again not necessary to compare moderator density profiles.

For the reader to have an idea of the power distribution inside the studied 3×3 fuel assembly cluster, the pin powers computed with Serpent 2/SUBCHANFLOW are depicted in Fig. 13. To improve readability only 8 horizontal cuts through the minicore are displayed. The power is slightly shifted into the lower half of the minicore. Furthermore, the unpoisoned UOX fuel assemblies produce significantly more power than the MOX ones which include wet annular burnable absorber (WABA) rods.

The fact that the minicore has one symmetry axis in radial direction can be used to test the quality and convergence of the Monte Carlo solution. Evaluated based on the pin power distribution, the maximal relative difference in the Serpent 2/SUBCHANFLOW solution between two symmetry calculation nodes is $3.4 \cdot 10^{-3}$. As powers are not available for the MCNP5/SUBCHANFLOW solution, the effective Doppler temperature distribution was used. A maximal deviation between symmetry positions of $5.6 \cdot 10^{-3}$ was detected. In both cases, the found asymmetry in the solution is larger than alleged convergence of the coupled solution.

In a next step, the 3D effective Doppler and moderator temperature distributions as computed by Serpent 2/SUBCHANFLOW and MCNP5/SUBCHANFLOW were benchmarked. A maximum absolute difference in Doppler temperature for all nodes of both models of 26 K was found. Locally, this corresponds to a relative difference in Doppler temperature of 2.8%. The absolute differences in Doppler and moderator temperatures in Kelvin between SSS2/SCF and MCNP5/SCF solutions for five vertical cuts through the minicore are displayed in Fig. 14. In this figure, index i denotes fuel pin positions in x-direction. It runs from 0 to 50. Likewise, index j represents fuel pin positions in y-direction, having the same value range. All absolute differences were obtained by subtracting the Serpent 2/SUBCHANFLOW solution from the one of the MCNP5/SUBCHANFLOW.

In the lower and axial sections of the minicore, the difference in Doppler temperature is larger in the MOX assemblies (see Fig. 14(b)). MCNP5/SUBCHANFLOW predicts the fuel there to be effectively hotter. In the vicinity of the middle of the minicore, however, the most pronounced differences appear in the UOX fuel assemblies. Which in turn Serpent 2/SUBCHANFLOW evaluates to be hotter.

The absolute differences in moderator temperature show the same generic behavior as the Doppler temperature. Only for the vertical slices for $i = 9$ and $i = 26$, two vertical lines of pronounced differences can be seen that have no correspondence in the Doppler temperature differences. These were found to be caused

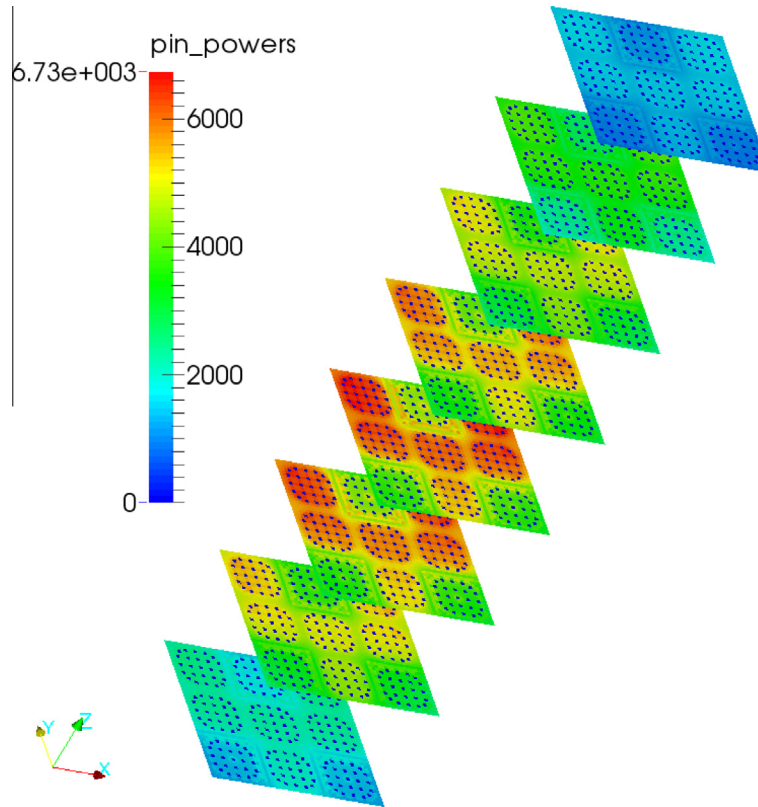


Fig. 13. Pin power distribution in Watts as predicted by Serpent 2/SUBCHANFLOW.

by a different modeling of the sub-channels between fuel assemblies. As the minicore exhibits strong power gradients along the $i = 9$ and $i = 26$ planes, the differences in modeling only became clearly visible in these two cases.

As both coupled codes use the same sub-channel thermal-hydraulics tool and it has been checked that the thermal-hydraulic models especially the closure relations used are comparable, the observed differences in effective Doppler temperature and moderator temperatures can be attributed to deviations in the neutron transport model.

Like in the channel thermal-hydraulics benchmark against TRIPOLI4/SUBCHANFLOW, in both cases JEFF 3.1.1 CE nuclear data was employed but processed differently. Moreover, the internal coupling of MCNP5/SUBCHANFLOW also applied the pseudo material approach. However, the adapted MCNP5 version interpolates $S(\alpha, \beta)$ tables on-the-fly with an advanced interpolation scheme. Additionally, it has to be pointed out that MCNP5 has probability table treatment for the unresolved resonance range on by default. As the use of probability tables is not yet compatible with Serpent 2's TMS method, the unresolved resonance range of all included nuclides were neglected. Finally, unlike Serpent 2/SUBCHANFLOW the temperature of the cladding and the gas in fuel rod gap are not updated by MCNP5/SUBCHANFLOW (Ivanov et al., 2014). They are kept at hot zero power conditions.

4. Demonstration of full PWR coupled calculation and assessment of numerical performance

In the second exercise of the OECD/NEA and U.S. NRC PWR MOX/UO₂ core transient benchmark, a 3D hot full power scenario is to be computed. For the layout of the PWR core in question please refer to Fig. 3. The corresponding operating conditions are summarized in Table 8. The critical boron concentration is to be determined.

To be able to perform the critical boron search, SSS2/SCF was extended. The critical boron search is realized as a loop over coupled Monte Carlo neutron transport and thermal-hydraulics simulations. The relation to estimate the new soluble poison concentration is given in Eq. (11). Serpent 2 adjusts the boron concentration in materials flagged as coolant in the internal coupling to SUBCHANFLOW. Thereafter, it recomputes all macroscopic and majorant cross sections needed by the transport simulation with thermal-hydraulic feedback. For the first iteration, a guess of the slope dc_b/dk_{eff} is required. It has to be given as an input by the user. In later iterations, the slope is evaluated based on previous simulation results.

$$c_{b,i} = c_{b,i-1} - (k_{\text{eff}} - 1) \frac{dc_b}{dk_{\text{eff}}} \quad (11)$$

The stopping criterion for the critical boron search is shown in Eq. (12). This criterion considers that the SSS2/SCF solution is subject to statistical uncertainties that depend on the total number of neutron histories simulated as $\sigma_{k_{\text{eff}}}$ is the standard deviation of the tallied eigenvalue.

$$|k_{\text{eff}} - 1| < \sigma_{k_{\text{eff}}} \quad (12)$$

Serpent 2/SUBCHANFLOW is employed to model the active core of the PWR in question with two different spatial resolutions in the thermal-hydraulics model. One SSS2/SCF model uses channel level (CH) the other sub-channel level (SBCH) thermal-hydraulics. The purpose of having two Serpent 2/SUBCHANFLOW models with different resolution in the thermal-hydraulics domain is to evaluate the influence of the spatial resolution in that domain on steady-state simulation results.

The channel thermal-hydraulics model includes one channel per fuel assembly, i.e. 193 parallel laterally coupled channels in total. In axial direction, each channel is subdivided in 20 nodes. The fuel rods of each fuel assembly are represented by an average

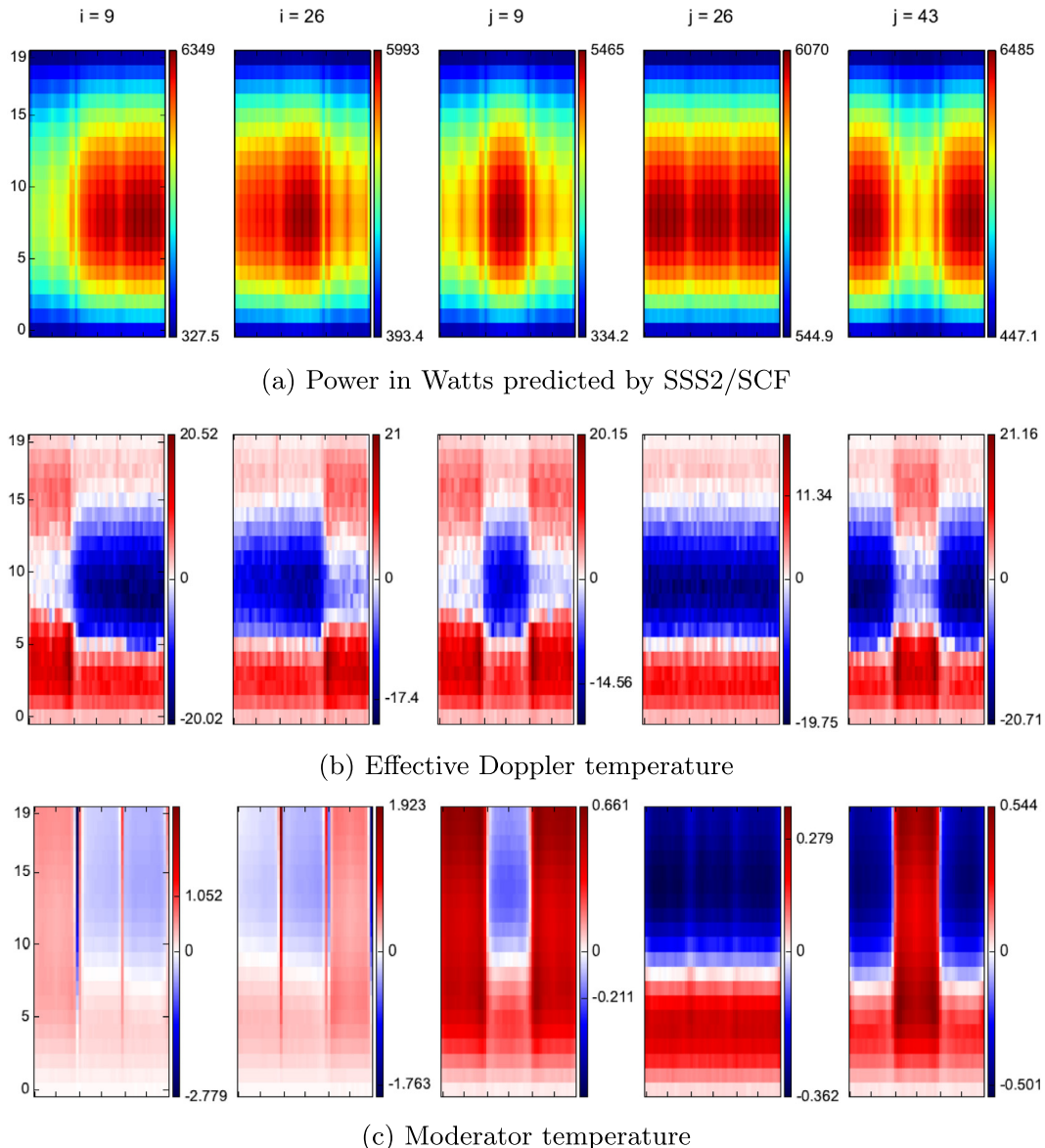


Fig. 14. Comparison of local power prediction by SSS2/SCF (a) and absolute difference in Doppler (b) and moderator temperatures (c) in Kelvin between MCNP5/SCF and SSS2/SCF solutions for five vertical cuts through the minicore.

Table 8

HFP operating conditions of OECD/NEA and U.S. NRC PWR MOX/UO₂ core transient benchmark.

Quantity	Value
Power	3565 MW
Core mass flow rate	15849.4 kg/s
Inlet pressure	15.5 MPa
Coolant inlet temperature	560 K

rod. For solving the heat conduction problem, this rod is radially discretized using 12 nodes. 10 of these nodes describe the fuel pellet and 2 nodes are left for gap and cladding. The thermo-physical properties of fuel and cladding material as well as the gap heat transfer coefficient are taken from the benchmark specifications (Kozlowski and Downar, 2003).

The sub-channel thermal-hydraulics model consists of 62,532 sub-channels divided into 35 axial mesh layers. All 55,777 fuel rods and guide tubes of the PWR core are modeled explicitly. Radially,

the discretization of each fuel rod is identical to the one of the average rod in the channel resolution model. The resultant sub-channel thermal-hydraulic model consists of 2.2 million cells in the fluid domain and 23.4 million in the solid domain.

ENDF/B VII.0 evaluated nuclear data is utilized. For Serpent 2's stochastic mixing fall back a 5 K spacing of thermal scattering data sets was chosen.

The Wielandt shift presented in subSection 2.4 is used to compute a well converged fission source the SSS2/SCF simulations can start from. Moreover, a power distribution produced by DYN SUB (Daeubler et al., in press; Gomez-Torres et al., 2012a,b), a deterministic reactor simulator, is used as initial power shape in SUBCHANFLOW. The local Doppler temperature and moderator density convergence targets are set to 0.5%. The convergence criterion for the effective multiplication factor is 5 pcm.

Per coupled iteration step, Serpent 2 modeled $4 \cdot 10^6$ neutrons per cycle. It was decided to employ 650 inactive cycles followed by 2500 active ones. The number of inactive cycles was chosen conservatively to ensure a converged fission source, assessed using

the Shannon entropy evaluated on a 5×5 mesh, and sufficient statistics for the UFS method. Furthermore, possible changes in the convergence behavior of the Monte Carlo simulation between different coupled iterations were also taken into account.

Furthermore, the authors wish to assess the quality of the coupled SSS2/SCF solutions obtained by analyzing the propagated statistical uncertainties of the coupled data fields, i.e. powers, fuel and moderator temperatures as well as coolant densities. 10 replica runs of both the CH and SBCH models are performed. After the runs have finished, the spread of the results is analyzed using statistical methods to estimate the propagated uncertainties.

For the hot full power exercise no reference transport solution exists in the benchmark. Consequently, a pin-homogenized/sub-channel DYNSUB calculation was performed to have an alternative higher spatial resolution result. A comparison of the critical boron concentration and the core average thermal-hydraulic properties is given in Table 9. The statistical uncertainties quoted on the SSS2/SCF results in this table were based on the 10 replica runs. All original nodal benchmark results presented in Table 9 were taken from the final benchmark report (Kozlowski and Downar, 2007).

Both the low order deterministic DYNSUB as well as Serpent 2/SUBCHANFLOW produce a significantly lower critical boron concentration than the nodal benchmark solutions. The corresponding lower core multiplication of the pin-by-pin solutions is in line with the observations made for the 2D HZP case which was studied to test the Wielandt shift implementation (refer to Table 10). The eigenvalue predicted by Serpent matches that of the “reference” DeCART solution of the original benchmark very well, however, the differences in assembly powers are larger than between DeCART and MCNP. The DeCART solution used the method of characteristics employing a 47G cross section library produced with HELIOS. DeCART like Serpent modeled the heterogeneity of each fuel pin cell. The differences can be attributed to energy discretization and cross section evaluation. Deviations between MCNP and Serpent for this benchmark exercise are due to differences in cross sections. MCNP used ENDF/B VI. Employing ENDF/B VI nuclear data Serpent estimates the eigenvalue to be 1.05705 ± 0.00001 and assembly power errors are very close to the values for MCNP.

The core average thermal-hydraulic properties match benchmark contributions well (cp. Table 9). Only the core average Doppler is found to be slightly lower than all other benchmark values. The benchmark definition specifies a correlation to compute effective Doppler temperature, heat capacity and thermal conductivity for both fuel and cladding as well as the heat transfer coefficient for the gas gap. As a consequence, differences in calculated Doppler temperatures can be partially attributed to code specific correlations to compute the heat transfer from cladding to coolant. Moreover, the numerical method and radial discretization for solving the heat conduction problem in the fuel rods play a role.

Table 10

Comparison of eigenvalues and assembly power errors for 2D cases of the OECD/NEA and U.S. NRC PWR MOX/UO₂ core transient benchmark, PWE refers to power-weighted error and EWE to the error-weighted error (Kozlowski and Downar, 2007).

	Eigenvalue	Assembly power error	
		%PWE	%EWE
<i>Nodal</i>			
CORETRAN 1/FA	1.06387	1.06	1.69
CORETRAN 4/FA	1.06379	0.96	1.64
EPISODE	1.06364	0.96	1.64
NUREC	1.06378	0.96	1.63
PARCS 2G	1.06379	0.96	1.63
PARCS 4G	1.06376	0.90	1.42
PARCS 8G	1.06354	0.86	1.25
SKETCH-INS	1.06379	0.97	1.67
<i>Pin-by-pin</i>			
BARS	1.05826	1.29	1.92
DeCART	1.05852	Ref	Ref
DORT	1.06036	0.86	1.12
MCNP	1.05699	0.67	1.26
DYNSUB 8G SP3	1.05888	0.70	1.09
SSS2	1.05862 ± 0.00001	1.22	1.68

The agreement between the 8G pin-homogenized simplified transport solution of DYNSUB and SSS2/SCF's continuous energy Monte Carlo neutron transport in terms of critical boron concentration is to a degree surprising indicating that low order deterministic methods are capable of accurately describing this PWR core. Furthermore, no significant differences between the Serpent 2/SUBCHANFLOW solutions employing a channel and a subchannel resolution thermal-hydraulics model are noticed.

In Fig. 15, the axial power profiles produced by Serpent 2/SUBCHANFLOW with both thermal-hydraulics models are compared the PARCS 2G solution as a typical nodal benchmark solution. Moreover, the MCNP5/ATHLET simulation done by Bernat et al. (2012) and pin-by-pin DYNSUB one are included. The statistical uncertainty of the SSS2/SCF results is not shown in the plots as it was to small, well below 0.05% everywhere, to be sensibly visualized. It can be observed that the power profiles determined by coupled Monte Carlo thermal-hydraulics tools agree perfectly. The PARCS profile is slightly shifted to the upper part of the core. DYNSUB produces a profile very close to those of the Monte Carlo neutron transport based tools.

The corresponding radially averaged effective Doppler temperature profiles shown in Fig. 16, however, exhibit no such perfect match. All solutions agree reasonably well, but the following general observations can be made: Firstly, the MCNP5/ATHLET effective Doppler does not follow the shape of its axial power profile. The reason for this behavior is unknown to the authors. Secondly, the temperature profiles computed by PARCS and SSS2/

Table 9
Comparison of critical boron concentration and core average thermal-hydraulic properties for the 3D HFP case of the OECD/NEA and U.S. NRC PWR MOX/UO₂ core transient benchmark.

	Critical c_b [ppm]	Average T_{Dopp} [K]	Average ρ_M [kg/m ³]	Average T_M [K]	Outlet ρ_M [kg/m ³]	Outlet T_M [K]
<i>Nodal</i>						
CORETRAN 1/FA	1647	908.4	706.1	581.0	658.5	598.6
CORETRAN 4/FA	1645	908.4	706.1	581.0	658.5	598.6
EPISODE	1661	846.5	701.8	582.6	697.4	585.5
NUREC	1683	827.8	706.1	581.1	661.5	598.7
PARCS 2G	1679	836.0	706.1	581.3	662.1	598.8
PARCS 4G	1674	836.1	706.1	581.3	662.1	598.8
PARCS 8G	1672	836.2	706.1	581.3	662.1	598.8
SKETCH-INS	1675	836.6	705.5	580.9	659.6	598.9
<i>Pin-by-pin</i>						
DYNSUB 8G SP3	1600	824.3	705.1	580.6	660.5	599.4
SSS2/SCF CH	1599 ± 0.23	824.6 ± 0.006	702.8 ± 0.010	582.5 ± 0.005	660.5 ± 0.005	599.2 ± 0.001
SSS2/SCF SBCH	1598 ± 0.21	824.4 ± 0.005	703.6 ± 0.011	582.05 ± 0.005	660.1 ± 0.005	599.1 ± 0.001

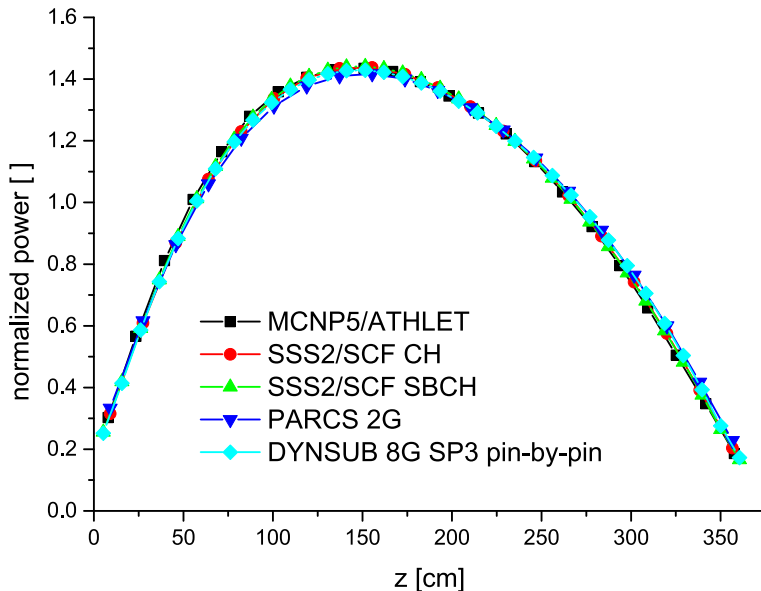


Fig. 15. Comparison of normalized axial power profiles.

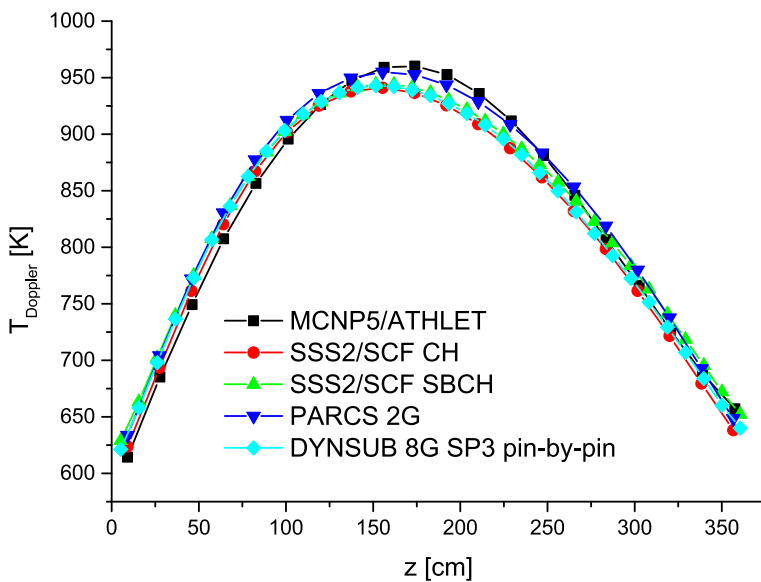


Fig. 16. Comparison of radially averaged effective Doppler temperatures.

SCF are very similar in shape but the maximal effective Doppler temperature seen by Serpent 2 is 944.2 K for the subchannel and 941.0 K for channel TH model as opposed to 954.9 K for PARCS – a significant difference as SSS2/SCF Doppler temperatures exhibit a maximum statistical uncertainty of 0.1 K. On top of the modeling differences pointed out during the discussion of differences in core average Doppler temperatures, PARCS employed the thermal conductivity of uranium oxide also for mixed uranium plutonium oxides. Its thermal-hydraulics model unlike SUBCHANFLOW considered no cross flows between fuel assemblies. The DYNSUB pin-by-pin solution follows the SSS2/SCF ones closely. The core wide averages of the effective Doppler temperature listed in Table 9 show the same trend.

Daeubler et al. (in press) also used DYNSUB with a nodal/channel thermal-hydraulic resolution to study the second exercise of the OECD/NEA and U.S. NRC PWR MOX/UO₂ core transient benchmark. The core average Doppler temperatures and axial Doppler

temperature profiles are found to be slightly lower than other benchmark solutions but very comparable to the values and behavior presented here for SSS2/SCF and DYNSUB pin-by-pin/subchannel. It may be concluded that the observed differences are mostly due to the different thermal-hydraulic codes used since all simulations using SUBCHANFLOW agree very well regardless of spatial resolution and transport approximation in their neutronics models.

In a next step, the radial power and moderator temperature profiles of SSS2/SCF with channel thermal-hydraulics model and PARCS 2G are compared. The relative differences in radial power are depicted in Fig. 17. It is worth to note that the PARCS 2G solution is perfectly eightfold symmetric. The distribution of relative differences, however, is not. It displays the residual asymmetry of the Serpent 2/SUBCHANFLOW results. The latter is below 0.5% in the entire domain. The asymmetry is statistically significant as it is up to two times larger than the statistical uncertainty estimated from the replica runs. Moreover, it can be observed that Serpent 2/

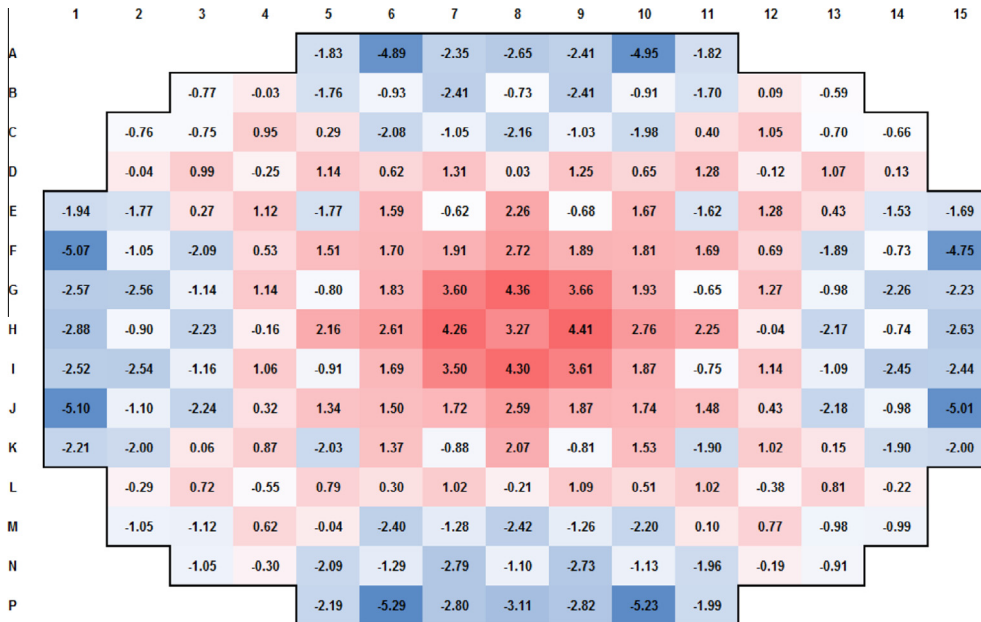


Fig. 17. Relative differences between assembly powers computed by SSS2/SCF CH and PARCS 2G.

SUBCHANFLOW predicts higher assembly powers at the center of the core and lower at the periphery. For a pure 2D neutronics problem under hot zero power conditions the trend is opposite and differences are smaller (see Fig. 18). The latter differences are rooted in the different methods for solving the neutron transport problem: 2G nodal diffusion for PARCS and continuous energy Monte Carlo neutron transport for SSS2. For the hot full power case, thermal-hydraulic models in PARCS and SUBCHANFLOW exhibit some differences as was discussed earlier. Moreover, PARCS employs a branched 2G effective homogenized cross section library modeling fuel temperature and moderator density dependence of cross sections with 3 points each. In between state points PARCS linearly interpolates its cross sections. The latter methodology roughly approximates the temperature dependence of macroscopic cross sections. Serpent 2/SUBCHANFLOW, however, employs TMS to continuously vary its continuous energy cross sections with temperature for all materials except water. Water is treated using the stochastic mixing approach with a temperature resolution of 5 K. The combination of these modeling differences leads to increasing differences and a change in their trend going from hot zero to hot full power conditions.

The relative differences in axially averaged moderator temperatures follow the same trend as the assembly powers (Fig. 19). Serpent 2/SUBCHANFLOW's residual asymmetry in assembly powers has a small influence on the moderator temperature profiles. These only exhibit tilts below 0.02%.

As a final step in this analysis of the second exercise, the pin-by-pin/subchannel solutions fields determined with Serpent 2/SUBCHANFLOW and DYNSUB 8G SP3 are to be benchmarked. The pin power distribution obtained with the SSS2/SCF SBCH is depicted in Fig. 20. The maximal local pin power difference between DYNSUB and Monte Carlo neutron transport based solution is 14.94% at the core periphery on axial layer 31. For this particular low power pin segment the estimated statistical uncertainty is 3.9%. At the core mid plane, the maximal local deviation in pin power is 7.57%. Here, the statistical uncertainty is 2.18%.

The overall distribution of local pin power differences at the core mid plane is shown in Fig. 21. For most of the axial layer the pin powers predicted by DYNSUB 8G SP3 fall within 2.5% of the Serpent 2/SUBCHANFLOW solution. DYNSUB computes pin

powers to be higher in the second and third batch assemblies in the central region of the core. SSS2/SCF sees higher pin powers in the ring of first batch UOX fuel assemblies near the outer boundary of the core.

Taking a closer look at the 2D projection in Fig. 21 reveals the tilt of the Monte Carlo power tally which is in the order of 3.0% between fuel pins in symmetry positions. This is larger than the estimated statistical uncertainty between 0.73% and 1.52% per cent in the affected regions.

After the pin powers also the thermal-hydraulic fields were compared. The maximal local pin power difference translates into a maximal change in local effective Doppler temperature by 3.97%. In the core mid plane, this maximal difference is slightly lower, i.e. 3.25%. As was observed for the channel level thermal-hydraulics models, the local moderator temperature is quite insensitive to local power and Doppler temperature deviations. The maximal relative difference between DYNSUB and SSS2/SCF is as low as 0.503%. In the core mid plane it drops to 0.29%.

The results obtained with Serpent 2/SUBCHANFLOW for second exercise of the OECD/NEA and U.S. NRC PWR MOX/UO₂ core transient benchmark were found to be satisfactory in terms of physics. For a routine application of the coupled code, however, its numerical performance is of utmost importance. The full PWR core critical boron concentration search simulation consumed 3.7 CPU-years for the channel and 5.8 CPU-years for the subchannel thermal-hydraulics resolution. Both calculations were run on KIT SCC's IC2 cluster which consists of Intel Xeon E5-2670 nodes interconnected with InfiniBand.

The authors took the channel and subchannel thermal-hydraulics models for the 3D hot full power exercise of the OECD/NEA and U.S. NRC PWR MOX/UO₂ core transient benchmark and looked at speed up S (Eq. (13)) as well as parallel efficiency E (Eq. (14)) achieved on the IC2 cluster. Both quantities were measured relative to the execution on one compute node, i.e. 16 cores.

$$S(N) = \frac{T_{\text{elapsed, parallel}}}{T_{\text{elapsed, serial}}} \quad (13)$$

with N being the number of used compute nodes.

$$E(N) = \frac{S(N)}{N} \quad (14)$$

	1	2	3	4	5	6	7	8	9	10	11	12	13	14	15
A					0.73	-2.29	-0.15	-0.81	-0.16	-2.27	0.80				
B				1.18	1.80	0.64	0.69	-0.39	0.58	-0.29	0.79	0.73	1.78	1.09	
C			1.05	1.40	1.87	0.91	-1.03	-0.73	-1.42	-0.70	-0.91	0.98	1.85	1.36	1.14
D			1.78	1.85	-0.21	0.57	-0.28	0.07	-1.17	0.08	-0.26	0.60	-0.15	1.87	1.89
E		0.70	0.64	0.90	0.59	-2.46	-0.21	-2.09	0.04	-2.07	-0.15	-2.39	0.63	1.01	0.84
F		-2.28	0.69	-1.07	-0.27	-0.18	-0.85	-1.14	-0.41	-1.07	-0.75	-0.10	-0.14	-0.85	0.93
G		-0.09	-0.32	-0.71	0.14	-2.07	-1.11	0.12	0.82	0.20	-1.00	-1.95	0.27	-0.49	0.01
H		-0.66	0.68	-1.39	-1.09	0.12	-0.36	0.80	-0.37	0.89	-0.29	0.25	-0.93	-1.21	0.92
I		0.06	-0.16	-0.57	0.23	-1.95	-1.01	0.19	0.86	0.24	-0.92	-1.79	0.35	-0.47	-0.04
J		-1.97	1.02	-0.73	-0.06	-0.03	-0.62	-0.96	-0.26	-0.91	-0.59	0.09	0.04	-0.74	1.00
K		1.02	1.00	1.21	0.81	-2.22	0.01	-1.91	0.25	-1.86	0.05	-2.18	0.80	1.16	0.89
L		2.14	2.15	0.08	0.79	-0.10	0.29	-0.93	0.28	-0.04	0.79	0.03	2.05	1.97	
M		1.48	1.70	2.11	1.12	-0.85	-0.59	-1.29	-0.52	-0.78	1.11	2.02	1.54	1.24	
N		1.42	2.00	0.77	0.82	-0.24	0.71	-0.18	0.93	0.88	1.96	1.24			
P				0.82	-2.19	-0.04	-0.67	0.04	-2.11	0.88					

Fig. 18. Relative differences between assembly powers computed by SSS2 CH and PARCS 2G for the 2D HZP exercise.

	1	2	3	4	5	6	7	8	9	10	11	12	13	14	15
A					0.21	0.17	0.15	0.23	0.15	0.17	0.21				
B			0.25	0.24	0.04	0.06	0.02	0.07	0.02	0.06	0.04	0.24	0.26		
C		0.26	0.08	0.11	0.20	0.12	0.29	0.09	0.29	0.12	0.21	0.11	0.09	0.26	
D		0.24	0.11	0.37	0.18	0.30	0.19	0.38	0.19	0.30	0.19	0.37	0.11	0.24	
E		0.21	0.04	0.21	0.18	0.33	0.23	0.27	0.24	0.27	0.23	0.33	0.19	0.21	0.21
F		0.17	0.06	0.12	0.30	0.23	0.32	0.38	0.38	0.38	0.33	0.23	0.30	0.12	0.07
G		0.15	0.01	0.29	0.18	0.26	0.38	0.39	0.38	0.39	0.38	0.27	0.19	0.29	0.02
H		0.23	0.06	0.09	0.37	0.23	0.37	0.37	0.53	0.38	0.38	0.24	0.37	0.09	0.07
I		0.15	0.01	0.29	0.18	0.26	0.37	0.38	0.37	0.39	0.38	0.26	0.18	0.29	0.01
J		0.16	0.05	0.11	0.28	0.21	0.31	0.37	0.37	0.38	0.32	0.22	0.29	0.11	0.06
K		0.21	0.03	0.20	0.17	0.31	0.21	0.25	0.23	0.26	0.22	0.32	0.18	0.20	0.03
L		0.23	0.10	0.36	0.17	0.28	0.18	0.36	0.18	0.29	0.18	0.37	0.11	0.24	
M		0.25	0.07	0.10	0.19	0.10	0.28	0.08	0.28	0.11	0.20	0.10	0.08	0.25	
N		0.25	0.23	0.03	0.04	0.00	0.05	0.00	0.05	0.03	0.03	0.24	0.25		
P				0.21	0.16	0.14	0.22	0.14	0.16	0.21					

Fig. 19. Relative differences between axially averaged moderator temperatures computed by SSS2/SCF CH and PARCS 2G.

The results of the speed up measurements are displayed in Fig. 22. SSS2/SCF behaves well for the channel thermal-hydraulics model. If there was no communication overhead and no remaining serial or non-scaling fraction of the code, the theoretical maximum speed up at 2048 cores or 128 nodes would be 128 relative to the execution one node. A speed-up of 96.4 was determined experimentally for the latter case.

The subchannel thermal-hydraulics Serpent 2/SUBCHANFLOW model of the full PWR core does considerably worse. As the sub-channel thermal-hydraulics is far more expensive to solve than the channel level one (32 CPUh vs 8 CPUmin), the parallel speed up levels off much earlier. This is reflected by the parallel efficiency shown in Fig. 23. While SSS2/SCF CH model still achieves a parallel efficiency of 78% when running on 128 compute nodes, the efficiency of the SBCH model has plunged to a mere 29%.

As a tool to provide high-fidelity pin-resolved reference solution Serpent 2/SUBCHANFLOW should be employed with subchannel thermal-hydraulics models. The fact that SUBCHANFLOW does not scale with the hybrid-parallel Serpent 2 Monte Carlo code, prohibits a routine application. As a consequence, a domain decomposition methodology has to be introduced into SUBCHANFLOW in the near future. The successful implementation of a domain decomposition in subchannel thermal-hydraulics code COBRA-TF within the framework of the CASL project ([Salko et al., in press](#)) will serve as a reference for the authors' efforts.

Once this has been accomplished extending the coupling of Serpent 2 and SUBCHANFLOW to the burn-up mode of Monte Carlo tool can be considered. To handle the terabyte tallies ([Smith and Forget, 2013](#)) associated with full core pin-by-pin burn-up, also a form of domain decomposition will have to be

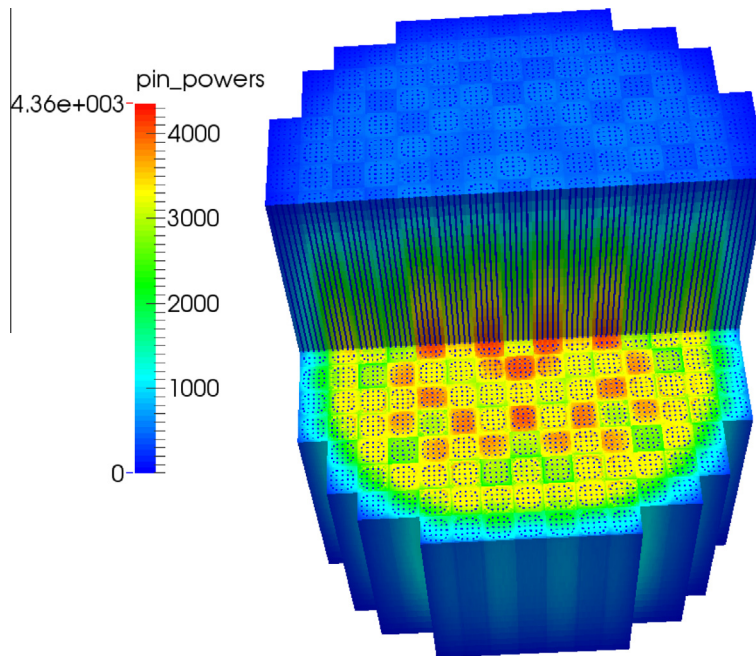


Fig. 20. Pin power distribution in Watts as predicted by SSS2/SCF SBCH.

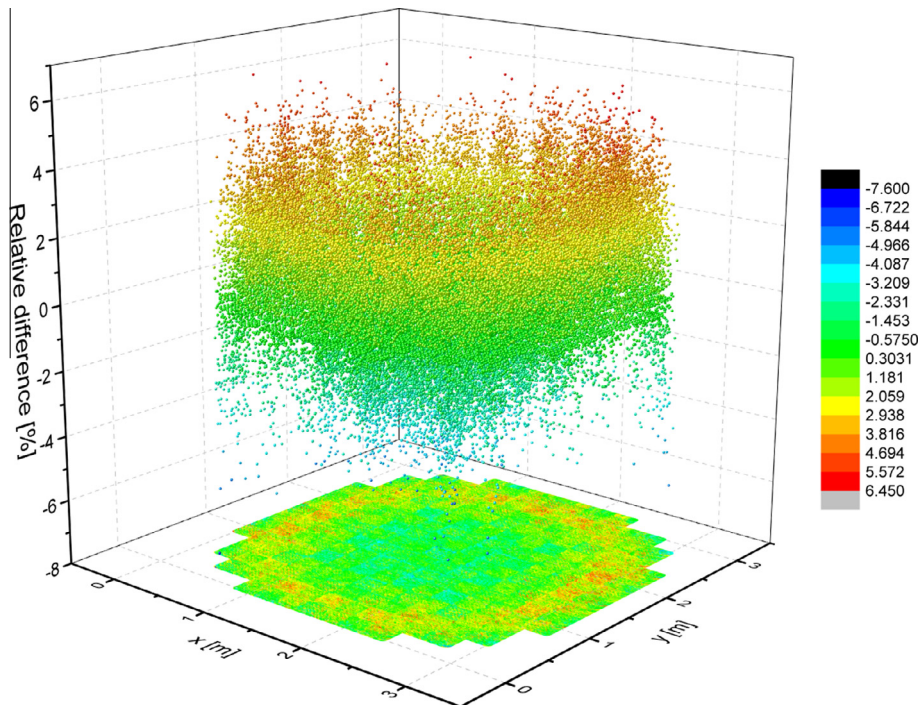


Fig. 21. Relative difference in pin powers between SSS2/SCF SBCH and DYNSUB at the core mid plane.

implemented in Serpent 2 to enable doing core follow calculations on clusters like IC2. On IC2, each compute node with 16 cores has only 64 GB main memory. Similar conclusions have been drawn by Horelik et al. (2014) and Mervin et al. (2012) who work on domain decompositions methodologies in the Monte Carlo neutron transport codes OpenMC and Shift respectively. With domain decomposition the issue of load balancing becomes more pressing. Even the SSS2/SCF simulations discussed beforehand were not perfectly load balanced since the length of a neutron history is a distributed quantity. In a domain decomposed situation, different sub-domains may have very different physical properties leading

to a significant imbalance of computational load. With the decomposition, methodologies to balance the load for Serpent 2/SUBCHANFLOW have to be developed.

5. First steps towards validation of Serpent 2/SUBCHANFLOW using BEAVRS cycle 1

The BEAVRS benchmark (Horelik et al., 2013) evolves around a commercial 3411 MW_{th} Westinghouse PWR reactor core. It includes the operation history for the first two cycles. Furthermore, measured

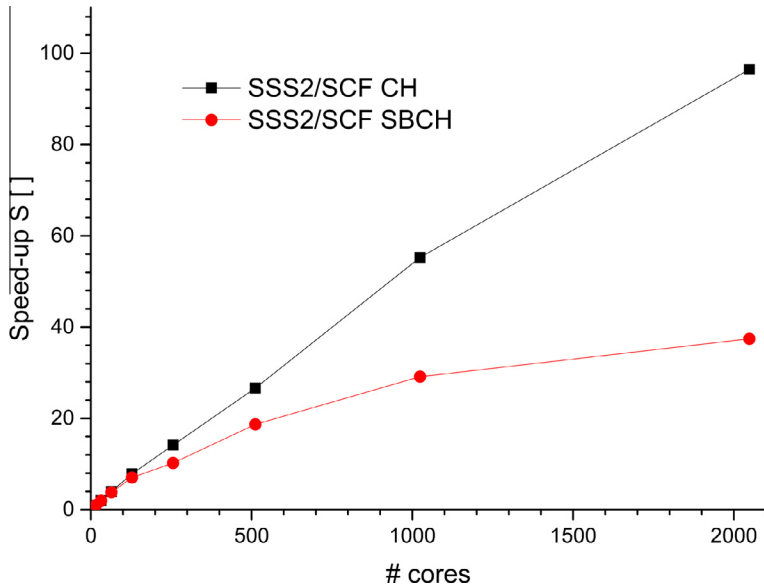


Fig. 22. Speedup of SSS2/SCF measured relative to execution on one node, i.e. 16 cores.

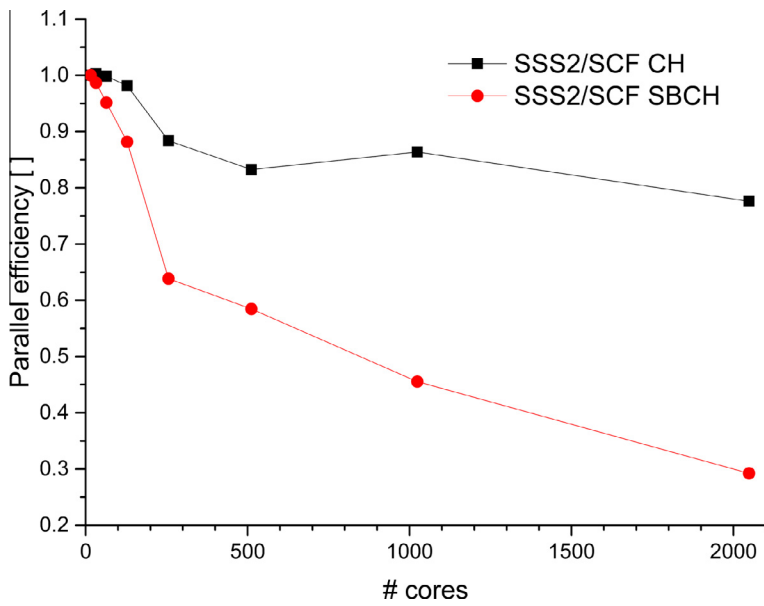


Fig. 23. Parallel efficiency of SSS2/SCF measured relative to execution on one node, i.e. 16 cores.

power distributions are available at a number of points in both cycles. Last but not least control rod bank worths were determined experimentally at the beginning of each of the two cycles.

The BEAVRS initial core was loaded with 17×17 fuel assemblies for three different enrichments: 1.6, 2.4 and 3.1 wt% U-235. To compensate the excess reactivity of the initial core, a total of 1266 burnable absorber pins are inserted into the guide tubes of fuel assemblies. Affected fuel assemblies are either loaded with 6, 12, 15, 16 or 20 such absorber pins. The control assemblies employ silver-indium-cadmium (AIC) as absorber material. They are grouped in 4 control (A,B,C,D) and 5 shutdown banks (SA,SB,SC,SD,SE). The loading pattern of the initial core and the configurations of inserted burnable absorber pins are shown in Fig. 24. The HZP operating conditions are summarized in Table 11. Under these conditions, all shutdown banks are fully withdrawn from the core.

Serpent 2/SUBCHANFLOW is used to model the active core of the PWR in question with a channel level thermal-hydraulics model. For total thermal power of 25 MW, strictly speaking, no TH model is necessary. The HZP case is analyzed with SSS2/SCF as a test for the coupling, the TMS temperature treatment and the stochastic mixing fall back. The obtained results are then compared to pure Monte Carlo neutron transport solutions produced with OpenMC and MC21 (Kelly et al., 2014).

The channel thermal-hydraulics model is very similar to the one used for the OECD/NEA and U.S. NRC PWR MOX/UO₂ core transient benchmark. 193 parallel channels consisting of 20 axial segments are used. Channel flow area, heated and wetted perimeters are adapted to correctly represent the BEAVRS fuel. Furthermore, the position of the spacer grids is changed to match the new layout. The form loss coefficient of the each spacer grid is assumed to be 1.0.

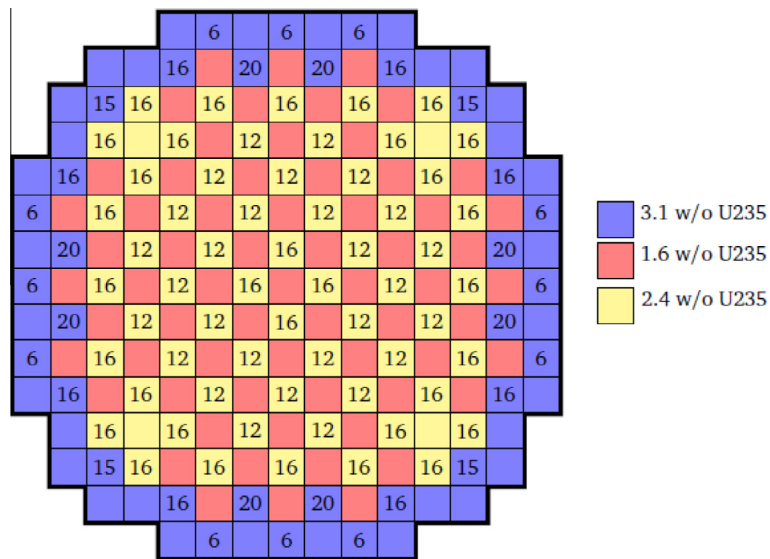


Fig. 24. Layout of the BEAVRS initial core.

Table 11
HZP operating conditions of BEAVRS initial core.

Quantity	Value
Power	25 MW
Core mass flow rate	15229.17 kg/s
Outlet pressure	15.5 MPa
Coolant inlet temperature	566 K
CR bank A	Step 228
CR bank B	Step 228
CR bank C	Step 228
CR bank D	Step 213
Critical boron	975 ppm

Once more, ENDF/B VII.0 evaluated nuclear data is employed. For Serpent 2's stochastic mixing fall back the 5 K spaced thermal scattering data sets of the OECD/NEA and U.S. NRC PWR MOX/UO₂ core transient benchmark are re-used. Like for the former case, a fission source file is produced with a Serpent 2 run utilizing Wielandt's method.

The convergence criteria for eigenvalue, local Doppler temperature and moderator density are identical to those for the second exercise of the OECD/NEA and U.S. NRC PWR MOX/UO₂ core transient benchmark. For each transport calculation, Serpent 2 employs $5 \cdot 10^6$ neutrons per cycle. Per Monte Carlo neutron transport calculation 1000 cycles are skipped. 3000 active cycles were executed thereafter. The number of inactive cycles was chosen conservatively to ensure a converged fission source, assessed using the Shannon entropy evaluated on a 5×5 mesh, and sufficient statistics for the UFS method.

The hot zero power physics data for the BEAVRS PWR core includes a number of measured critical boron concentrations (CBC) and the corresponding insertions of control and shutdown banks. The core multiplication predicted by SSS2/SCF for these cases is listed in Table 12. The results for the codes OpenMC and nTRACER were taken from Ryu et al. (2014). Serpent 2/SUBCHANFLOW solutions perform as well as the other high-fidelity neutronics simulations. OpenMC (Romano and Forget, 2013) is another Monte Carlo neutron transport code and nTRACER (Jung et al., 2013) a deterministic tool based on the method of characteristics as well as on-the-fly cross section processing.

In the case of control and shutdown banks fully withdrawn from the core, SSS2/SCF's eigenvalue is only 65 pcm from critical. For all rodded configuration, this bias is less than 227 pcm.

For the all rods out configuration, assembly powers have been measured in 58 locations throughout the core. First, the axially integrated power measurements are analyzed. They have been normalized such that average axially integrated power is unity. The measurement uncertainty has been estimated to be 3.7%. The relative differences between the Serpent 2/SUBCHANFLOW simulation and the measurements are displayed in Fig. 25. The maximum observed difference is -13.24% in assembly B13 and there is a noticeable tilt in the field of relative differences.

Independently obtained MC21 and OpenMC solutions for this case are reported in Kelly et al. (2014). For both tools, the maximal ($C/E - 1$) occurs also in assembly B13, -12.7% for MC21 and -13.5% for OpenMC. Furthermore, these two solutions exhibit the same tilt in relative differences. The measured detector signals are significantly greater than all three solutions in the lower right quadrant in the core and significantly lower in the upper left quadrant.

To illustrate how differences in axially integrated powers translate into axial power profiles, the profile in the assembly with the largest C/E relative error, i.e. B13, and the one in the assembly with smallest C/E relative error, i.e. B03, are shown in Figs. 26 and 27. While the power shape is well captured in assembly B13, the overall power level is not. In assembly B03, a very good agreement of calculated and experimentally determined power profile is observed. Like for B13, the flux suppression caused by the spacer grids are clearly visible.

Last but not least, measurements of the worth of all control rod and some of the shutdown banks were performed. The associated measurement uncertainties are not known to the authors. The worths computed with Serpent 2/SUBCHANFLOW are contrasted with the experimental results in Table 13. The MC21 values were taken from Kelly et al. (2013). Bank worths evaluated with OpenMC and nTRACER can be found in Ryu et al. (2014).

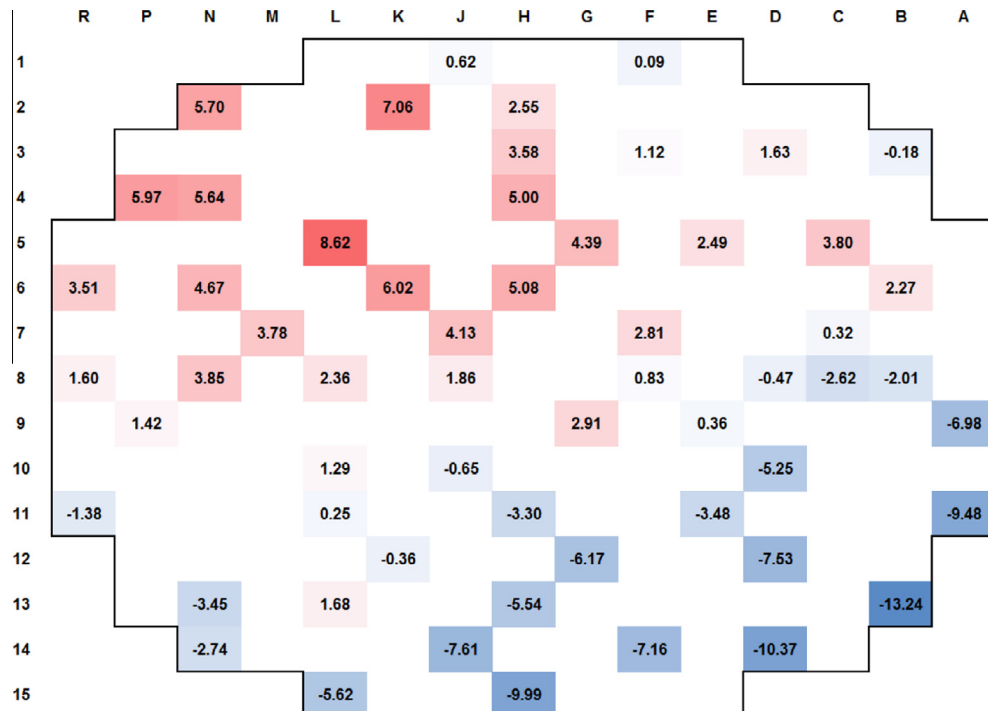
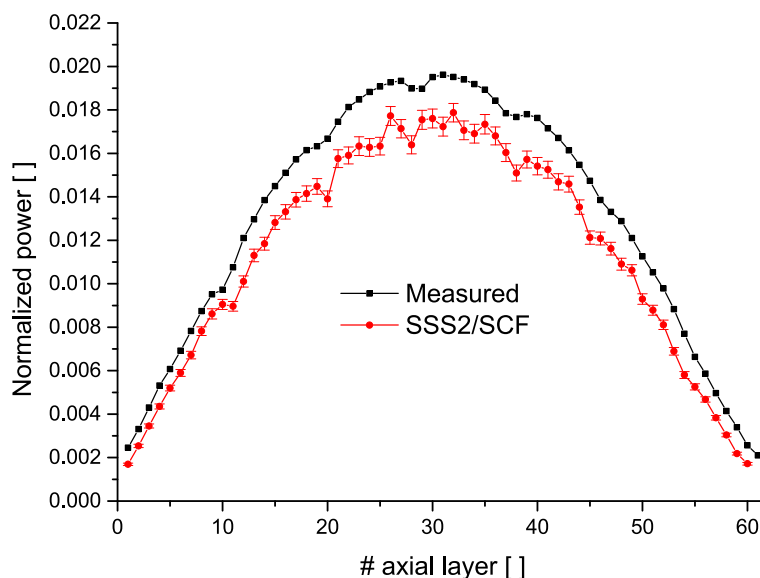
Except the worth of the D control rod banks, all worths are over-predicted by all tools relative to the measured values. The degree of over-prediction varies for banks and tools. For Serpent 2/SUBCHANFLOW, the maximum difference to the measured value occurs for the C control rod bank. The deviation is 63 pcm. All in all, the agreement between SSS2/SCF and the experimentally obtained bank worths is satisfactory.

It is the opinion of the authors that the BEAVRS model discussed above is sufficiently accurate to be the basis of validating the

Table 12

Cycle 1 criticality calculations vs measurements.

Case	Measured CBC [ppm]	OpenMC	nTRACER	SSS2/SCF
ARO	975	0.99920 ± 0.00004	0.99967	0.99935 ± 0.00001
D in	902	1.00080 ± 0.00004	1.00127	1.00127 ± 0.00003
CD in	810	1.00023 ± 0.00005	1.00068	1.00060 ± 0.00003
A,B,C,D in	686	0.99884 ± 0.00004	0.99931	0.99923 ± 0.00003
A,B,C,D,SE,SD,SC in	508	0.99725 ± 0.00004	0.99816	0.99774 ± 0.00003

Fig. 25. ($C/E - 1$) in per cent for HZP radial power distribution.Fig. 26. Comparison of axial power profiles in assembly with largest C/E relative error, i.e. B13.

Serpent 2/SUBCHANFLOW using cycle 1 and 2 plant data. The validation efforts are to proceed once the coupled code system has been extended to cover core follow calculations and its numerical performance has been improved enough to allow for finishing such

simulations in a reasonable amount of time. Moreover, the observed radial tilt in measured powers slowly disappears with burn-up in cycle 1. Measurements later in the cycle should compare better with simulations.

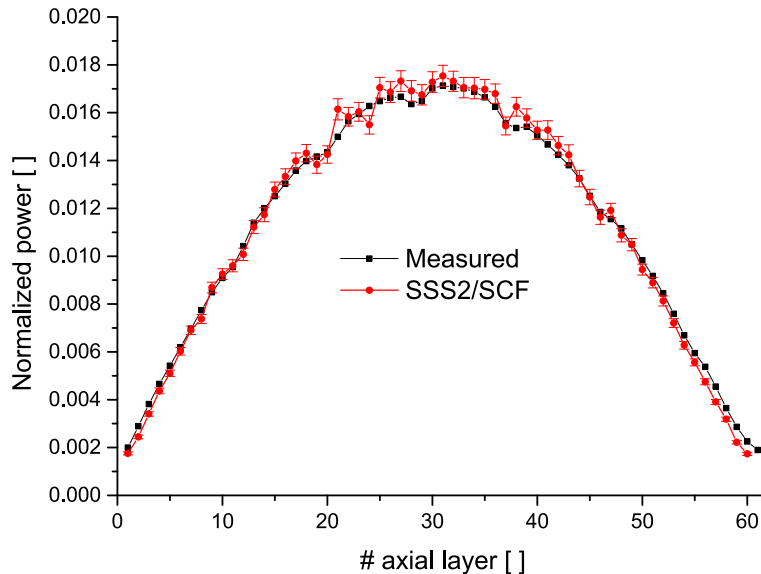


Fig. 27. Comparison of axial power profiles in assembly with smallest C/E relative error, i.e. B03.

Table 13

Cycle 1 HZP control rod bank worth comparison.

CR bank	Measured worth [pcm]	MC21 [pcm]	OpenMC [pcm]	nTRACER [pcm]	SSS2/SCF [pcm]
D	788	773	771 ± 6	782	776 ± 4
C	1203	1260	1234 ± 7	1229	1266 ± 5
B	1171	1172	1197 ± 7	1181	1198 ± 5
A	548	574	556 ± 6	584	594 ± 4
SE	461	544	501 ± 6	504	494 ± 4
SD	772	786	—	—	790 ± 4
SC	1099	1122	—	—	1109 ± 5

6. Conclusion and outlook

An internal coupling between the Monte Carlo code Serpent 2 and the sub-channel code SUBCHANFLOW has been developed. In order to verify the coupled Monte Carlo thermal-hydraulics code development, a code-to-code benchmark with the TRIPOLI4/SUBCHANFLOW and MCNP5/SUBCHANFLOW has been performed and a good agreement between the solutions has been found. Observed deviations can mostly be attributed to differences in coupling methodology and treatment of the temperature dependence of the CE nuclear data. The authors plan to quantitatively evaluate the different contributors to the deviations in the near future.

Furthermore, it was demonstrated that SSS2/SCF can be used to analyze realistic, industry-like cases by successfully completing exercise 2 of the OECD/NEA and U.S. NRC PWR MOX/UO₂ core transient benchmark. A detailed analysis of the obtained results, however, revealed that further work on improving the symmetry of the Monte Carlo tallies on an underlying symmetric geometry and fission source convergence needs to be done. Moreover, Serpent 2/SUBCHANFLOW's numerical performance was found to be satisfactory for channel thermal-hydraulics models but not for subchannel ones. This is mostly linked to the fact that SUBCHANFLOW lacks the capability to decompose its solution domain for execution on distributed memory architectures. The introduction of domain decomposition in SCF is planned for the near future.

In order to enable the simulation of reactor systems other than LWR and improve the description of the latter, achieving the compatibility of TMS with probability table sampling has a high priority.

Moreover, the authors plan to replace the stochastic mixing fall back for thermal bound-atom scattering with an on-the-fly

sampling of the thermal scattering data in the long term. Such an approach would go better with the TMS method and the concept of an internal coupling. To this end, it will be assessed how the methodology recently developed by Pavlou and Ji (2014) might be implemented in Serpent 2 and what accuracies may be achieved.

In this paper, early efforts to validate Serpent 2/SUBCHANFLOW simulations using the BEAVRS benchmark have been discussed. While the physics were well represented for the tests conducted at HZP, the core follow calculations can only be performed once Serpent 2/SUBCHANFLOW has been extended to cover burn-up calculations. To handle the terabyte tallies associated with full core pin-by-pin burn-up domain decomposition has to be implemented in Serpent 2. In a domain decomposed situation, different sub-domains may have very different physical properties leading to a significant imbalance of computational load. Methods to balance this load for the extended Serpent 2/SUBCHANFLOW have to be considered.

Furthermore, the long-term development plan for the Serpent 2/SUBCHANFLOW coupled code system includes coupled neutron-gamma transport with direct heating of structures and coolant as well as extending the coupling to transients once Serpent's dynamic simulation mode is mature. Currently, this dynamic mode cannot handle delayed neutrons yet (Leppänen, 2013a). Last but not least, the impact of modeling the actual radial power and temperature profiles in each fuel rod on a coupled neutronics thermal-hydraulics solution is to be analyzed – both in terms of physics and of computational resources consumed. The option of performing such simulations is to be added to the internal coupling of Serpent 2/SUBCHANFLOW so it can be employed by users whenever deemed necessary.

Acknowledgments

The authors wish to acknowledge the support of the Nuclear Safety Program for the research topic “multi-physics methods for LWR” and the Steinbuch Centre for Computing (SCC) of the Karlsruhe Institute of Technology (KIT). Additionally, the authors thank VTT Technical Research Center of Finland for their assistance concerning Serpent and for providing us with their BEAVRS core model.

This work has been co-funded by the European Commission and performed as part of the seventh EURATOM Framework Programme for nuclear research and training activities under HPMC-295971.

References

- Becker, B., Dagan, R., Lohnert, G., 2009. Proof and implementation of the stochastic formula for ideal gas, energy dependent scattering kernel. *Ann. Nucl. Energy* 36, 470–474. <http://dx.doi.org/10.1016/j.anucene.2008.12.001>.
- Bernnat, W., Buck, M., Mattes, M., Zwermann, W., Pasichnyk, I., Velkov, K., 2012. Coupled Monte Carlo neutronics and thermal hydraulics for power reactors. In: Proceedings of PHYSOR 2012 Conference, Knoxville, Tennessee.
- Brown, F., 2006. On the use of shannon entropy of the fission distribution for assessing convergence of Monte Carlo criticality calculations. In: Proceedings of the PHYSOR 2006 Conference, Vancouver, Canada.
- Brown, F., 2007. Wielandt acceleration for MCNP5 Monte Carlo eigenvalue calculations. In: Proceedings of M&C + SNA 2007 Conference.
- Cooper, J. et al., 2007. Revised Release on the IAPWS Industrial Formulation 1997 for the Thermodynamic Properties of Water and Steam. Technical Report. International Association for the Properties of Water and Steam.
- Daeubler, M., Jimenez, J., Sanchez, V., 2014. Development of a high-fidelity Monte Carlo thermal-hydraulics coupled code system serpent/SUBCHANFLOW – first results. In: Proceedings of PHYSOR 2014 Conference.
- Daeubler, M., Trost, N., Jimenez, J., Sanchez, V., Stieglitz, R., Macian-Juan, R., in press. Static and transient pin-by-pin simulations of a full PWR core with the extended coupled code system DYNSUB. *Ann. Nucl. Energy*. <http://dx.doi.org/10.1016/j.anucene.2014.09.057>.
- Dufek, J., Hoogenboom, J., 2014. Description of a stable scheme for steady-state coupled Monte Carlo-thermal-hydraulic calculations. *Ann. Nucl. Energy* 68, 1–3. <http://dx.doi.org/10.1016/j.anucene.2013.12.017>.
- Dumontel, E., Malvagi, F., Zoia, A., Mazzolo, A., Artusio, D., Dieudonné, C., Mulatier, C.D., 2014. Particle clustering in Monte Carlo criticality simulations. *Ann. Nucl. Energy* 63, 612–618. <http://dx.doi.org/10.1016/j.anucene.2013.09.008> <<http://www.sciencedirect.com/science/article/pii/S0306454913004787>>.
- Espel, F.P., Avramova, M.N., Ivanov, K.N., Misu, S., 2013. New developments of the MCNP/CTF/NEM/NJOY code system – Monte Carlo based coupled code for high accuracy modeling. *Ann. Nucl. Energy* 51, 18–26. <http://dx.doi.org/10.1016/j.anucene.2012.06.031>.
- Forget, B., Xu, S., Smith, K., 2014. Direct Doppler broadening in Monte Carlo simulations using the multipole representation. *Ann. Nucl. Energy* 64, 78–85. <http://dx.doi.org/10.1016/j.anucene.2013.09.043>.
- Gill, D., Aumiller, D., Griesheimer, D., 2014. Monte carlo and thermal-hydraulic coupling via PVMEXEC. In: Proceedings of PHYSOR 2014 Conference.
- Gomez-Torres, A.M., Sanchez-Espinoza, V.H., Ivanov, K., Macian-Juan, R., 2012a. DYNSUB: a high fidelity coupled code system for the evaluation of local safety parameters – Part I: Development, implementation and verification. *Ann. Nucl. Energy* 48, 108–122. <http://dx.doi.org/10.1016/j.anucene.2012.05.011>.
- Gomez-Torres, A.M., Sanchez-Espinoza, V.H., Ivanov, K., Macian-Juan, R., 2012b. DYNSUB: a high fidelity coupled code system for the evaluation of local safety parameters – Part II: Comparison of different temporal schemes. *Ann. Nucl. Energy* 48, 123–129. <http://dx.doi.org/10.1016/j.anucene.2012.05.033>.
- Horelik, N., Herman, B., Forget, B., Smith, K., 2013. Benchmark for evaluation and validation of reactor simulations (BEAVRS). In: Proceedings of M&C 2013 Conference, Sun Valley, Idaho.
- Horelik, N., Forget, B., Smith, K., Siegel, A., 2014. Domain decomposition and terabyte tallies with the OpenMC Monte Carlo neutron transport code. In: Proceedings of PHYSOR 2014 Conference, Kyoto, Japan.
- Ivanov, A., Sanchez, V., Stieglitz, R., Ivanov, K., 2013. High fidelity simulation of conventional and innovative LWR with the coupled Monte-Carlo thermal-hydraulic system MCNP-SUBCHANFLOW. *Nucl. Eng. Des.* 262, 264–275. <http://dx.doi.org/10.1016/j.nucengdes.2013.05.008>.
- Ivanov, A., Sanchez, V., Stieglitz, R., Ivanov, K., 2014. Internal multi-scale multi-physics coupled system for high fidelity simulation of light water reactors. *Ann. Nucl. Energy* 66, 104–112. <http://dx.doi.org/10.1016/j.anucene.2013.12.003>.
- Jung, Y.S., Joo, H.G., Yoon, J.I., 2013. Core follow calculation with the nTRACER numerical reactor and verification using power reactor measurement data. In: Proceedings of M&C 2013 Conference, Sun Valley, Idaho.
- Kelly, D., Sutton, T.M., Wilson, S., 2012. MC21 analysis of the nuclear energy agency Monte Carlo performance benchmark problem. In: Proceedings of PHYSOR 2012 Conference, Knoxville, Tennessee.
- Kelly, D., Aviles, B., Herman, B., 2013. MC21 analysis of the MIT PWR benchmark: hot zero power results. In: Proceedings of M&C 2013 Conference, Sun Valley, Idaho.
- Kelly, D., Aviles, B., Romano, P., Hermann, B., Horelik, N., Forget, B., 2014. Analysis of selected BEAVRS PWR benchmark cycle 1 results using MC21 and OpenMC. In: Proceedings of PHYSOR 2014 Conference.
- Kochuas, B., Stimpson, S., Collins, B., Downar, T., Brewster, R., Baglietto, E., Yan, J., 2012. Coupled full core neutron transport/CFD simulations of pressurized water reactors. In: Proceedings of PHYSOR 2012 Conference, Knoxville, Tennessee.
- Kozlowski, T., Downar, T.J., 2003. OECD/NEA and U.S. NRC PWR MOX/UO₂ Core transient benchmark – Final Specification. Technical Report. OECD Nuclear Energy Agency/Nuclear Science Committee.
- Kozlowski, T., Downar, T.J., 2007. OECD/NEA and U.S. NRC PWR MOX/UO₂ Core Transient Benchmark – Final Report. Technical Report. OECD Nuclear Energy Agency/Nuclear Science Committee.
- Leppänen, J., 2012. Modeling of nonuniform density distributions in the Serpent 2 Monte Carlo code. *Nucl. Sci. Eng.* 174, 318–325. <http://dx.doi.org/10.13182/NSE12-54>.
- Leppänen, J., 2013a. Development of a dynamic simulation mode in Serpent 2 Monte Carlo code. In: Proceedings of M&C 2013 Conference, Sun Valley, Idaho.
- Leppänen, J., 2013b. Serpent? A Continuous-energy Monte Carlo Reactor Physics Burnup Calculation Code. Technical Report. VTT Technical Research Centre of Finland.
- Leppänen, J., Viitanen, T., Valtavirta, V., 2012. Multi-physics coupling scheme in the Serpent 2 Monte Carlo code. *Trans. Am. Nucl. Soc.* 107, 1165–1168.
- Leppänen, J., Valtavirta, V., Aufiero, M., 2014. Unstructured mesh based multi-physics interface for CFD code coupling in the Serpent 2 Monte Carlo code. In: Proceedings of PHYSOR 2014 Conference, Kyoto, Japan.
- Li, L., Wang, K., 2012. The first-principle coupled calculations using TMCC and CFX for the pinwise simulation of LWR. In: Proceedings of PHYSOR 2012 Conference, Knoxville, Tennessee.
- Martin, W., Brown, F., Wilderman, S., Yesilyurt, G., 2013. On-the-fly neutron Doppler broadening in MCNP. In: SNA + MC 2013 – Joint International Conference on Supercomputing in Nuclear Applications + Monte Carlo.
- Mattes, M., Keinert, J., 2005. Thermal Neutron Scattering Data for Moderator Materials H2O, D2O and ZrHx in the ENDF-6 Format and as ACE Library for the MCNP(X) Codes. Technical Report INDC(NDS)-0470. International Atomic Energy Agency.
- Mervin, B.T., Mosher, S.W., Evans, T.M., Wagner, J.C., Maldonada, G.I., 2012. Variance estimation on domain decomposed Monte Carlo eigenvalue calculations. In: Proceedings of PHYSOR 2012 Conference, Knoxville, Tennessee.
- ORNL, 2011. Scale: A Comprehensive Modeling and Simulation Suite for Nuclear Safety Analysis and Design. Technical Report ORNL/TM-2005/39.
- Pavlou, A.T., Ji, W., 2014. On-the-fly sampling of temperature-dependent thermal neutron scattering data for Monte Carlo simulations. *Ann. Nucl. Energy* 71, 411–426. <http://dx.doi.org/10.1016/j.anucene.2014.04.028>.
- Romano, P.K., Forget, B., 2013. The openmc Monte Carlo particle transport code. *Ann. Nucl. Energy* 51, 274–281. <http://dx.doi.org/10.1016/j.anucene.2012.06.040> <<http://www.sciencedirect.com/science/article/pii/S0306454912003283>>.
- Ryu, M., Jung, Y., Cho, H., Joo, H., 2014. Solution of the BEAVRS benchmark using the nTRACER direct whole core transport code. In: Proceedings of PHYSOR 2014 Conference.
- Salko, R., Schmidt, R., Avramova, M., in press. Optimization and parallelization of the thermal-hydraulic subchannel code CTF for high-fidelity multi-physics applications. *Ann. Nucl. Energy*. <http://dx.doi.org/10.1016/j.anucene.2014.11.005>.
- Sanchez, V., Imke, U., Ivanov, A., Gomez, R., 2010. SUBCHANFLOW: a thermal-hydraulic sub-channel program to analyse fuel rod bundles and reactor cores. In: Proceedings of the 17th Pacific Basin Nuclear Conference.
- Sjenitzer, B., 2013. The Dynamic Monte Carlo Method for Transient Analysis of Nuclear Reactors (Ph.D. thesis). Delft University of Technology.
- Sjenitzer, B.L., Hoogenboom, J.E., Escalante, J.J., Espinoza, V.S., 2015. Coupling of dynamic Monte Carlo with thermal-hydraulic feedback. *Ann. Nucl. Energy* 27–39. <http://dx.doi.org/10.1016/j.anucene.2014.09.018> <<http://www.sciencedirect.com/science/article/pii/S0306454914004903>>.
- Smith, K., Forget, B., 2013. Challenges in the development of high-fidelity LWR core neutronics tools. In: Proceedings of M&C 2013 Conference, Sun Valley, Idaho.
- Trumbull, T.H., 2006. Treatment of nuclear data for transport problems containing detailed temperature distributions. *Nucl. Technol.* 156, 75–86.
- Trumbull, T., Fieno, T., 2012. Temperature interpolation of thermal neutron incoherent inelastic scattering data in Monte Carlo calculations. In: Transactions of the American Nuclear Society, San Diego, CA.
- van der Marck, S., Meulekamp, R., Hogenbirk, A., 2005. New temperature interpolation in MCNP. In: Proceedings of M&C 2005 Conference, Avignon, France.
- Vazquez, M., Tsige-Tamirat, H., Ammirabile, L., Martin-Fuertes, F., 2012. Coupled neutronics thermal-hydraulics analysis using Monte Carlo and sub-channel codes. *Nucl. Eng. Des.* 250, 403–411. <http://dx.doi.org/10.1016/j.nucengdes.2012.06.007>.
- Viitanen, T., Leppänen, J., 2012a. Explicit temperature treatment in the Monte Carlo neutron tracking routines? First results. In: Proceedings of PHYSOR 2012 Conference, Knoxville, Tennessee.
- Viitanen, T., Leppänen, J., 2012b. Explicit treatment of thermal motion in continuous-energy Monte Carlo tracking routines. *Nucl. Sci. Eng.* 171, 165–173. <http://dx.doi.org/10.13182/NSE11-36>.
- Viitanen, T., Leppänen, J., 2013. Optimizing the implementation of the target motion sampling temperature treatment technique? How fast can it get? In: Proceedings of M&C 2013 Conference, Sun Valley, Idaho.
- Weber, D.P., Sofu, T., Yang, W.S., Downar, T.J., Thomas, J.W., Zhong, Z., Cho, J.Y., Kim, K.S., Chun, T.H., Joo, H.G., Kim, C.H., 2007. High-fidelity light water reactor analysis with the numerical nuclear reactor. *Nucl. Sci. Eng.* 155, 395–408.